Title

Long-term tolerance to skin commensals is established neonatally through a specialized dendritic cell subgroup.

Journal

Immunity, 56(6)

Authors

Weckel, Antonin
Dhariwala, Miqdad
Ly, Kevin
et al.

Publication Date

2023-06-13

DOI

10.1016/j.immuni.2023.03.008

Peer reviewed

HHS Public Access

Author manuscript

Immunity. Author manuscript; available in PMC 2024 June 13.

Published in final edited form as:

Immunity. 2023 June 13; 56(6): 1239–1254.e7. doi:10.1016/j.immuni.2023.03.008.

Long term tolerance to skin commensals is established neonatally through a specialized dendritic cell subgroup

Antonin Weckel[1], **Miqdad O. Dhariwala**[1], **Kevin Ly**[1,2], **Victoria M. Tran**[1,2], **Oluwasunmisola T. Ojewumi**[1], **Julianne B. Riggs**[2], **Jeanmarie R. Gonzalez**[1,2], **Laura R. Dwyer**[1,2], **Joy N. Okoro**[1], **John M. Leech**[1,3], **Margot S. Bacino**[4], **Grace D. Cho**[1,5], **Geil Merana**[1,6], **Niroshana Anandasabapathy**[7,8], **Yosuke Kumamoto**[9,10], **Tiffany C. Scharschmidt**[1]

[1]University of California, San Francisco, Department of Dermatology, San Francisco, CA 94143, USA

[2]University of California, San Francisco, Biomedical Sciences Graduate Program, San Francisco, CA 94143, USA

[3]Current Affiliation: Pfizer Inc. New York, NY, 10017, USA

[4]University of California, San Francisco, Oral and Craniofacial Sciences Graduate Program, San Francisco, CA 94143, USA

[5]University of California, Los Angeles, Department of Infectious Diseases, Los Angeles, CA 90095, USA

[6]Current Affiliation: 23andMe, South San Francisco, CA, 94080, USA

[7]Department of Dermatology, Meyer Cancer Center, Englander Institute for Precision Medicine, Weill Cornell Medical College, New York, NY, USA

[8]Immunology and Microbial Pathogenesis Program, Weill Cornell Medical College, New York, NY, USA

Lead contact: Tiffany C. Scharschmidt tiffany.scharschmidt@ucsf.edu.

Author Contributions

A.W. and T.C.S. designed the studies and wrote the manuscript. A.W. performed the experiments and analyzed the data. M.O.D., K.L., V.M.T, O.T.O, J.B.R., J.R.G, L.R.D, J.N.O., J.M.L, M.S.B, G.D.C. and G.M. assisted with experiments. Y.K, and N.A. provided resources and input on experimental design. T.C.S. oversaw all study design and data analysis. All authors discussed results and commented on the manuscript.

Declaration of Interests

T.C.S. is on the Scientific Advisory Board of Concerto Biosciences. N.A. is on the Scientific Advisory Board for Shennon Biotech, and consults or lectures for 23andMe, Cellino Biotech, Janssen Pharmaceuticals, and Immunitas Therapeutics. Other authors have no competing interests.

Inclusion and Diversity

One or more of the authors of this paper self-identifies as an underrepresented ethnic minority in their field of research or within their geographical location. One or more of the authors of this paper self-identifies as a gender minority in their field of research. One or more of the authors of this paper received support from a program designed to increase minority representation in their field of research. While citing references scientifically relevant for this work, we also actively worked to promote gender balance in our reference list.

[9]Department of Pathology, Immunology and Laboratory Medicine, Rutgers New Jersey Medical School, Newark, NJ 07103, USA.

[10]Center for Immunity and Inflammation, Rutgers New Jersey Medical School, Newark, NJ 07103, USA.

Summary:

Early life establishment of tolerance to commensal bacteria at barrier surfaces carries enduring implications for immune health but remains poorly understood. Here we showed that tolerance in skin was controlled by microbial interaction with a specialized subset of antigen presenting cells. More particularly, CD301b$^+$ type 2 conventional dendritic cells (DC) in neonatal skin were specifically capable of uptake and presentation of commensal antigens for the generation of regulatory T (Treg) cells. CD301b$^+$ DC2 were enriched phagocytosis and maturation programs, while also expressing tolerogenic markers. In both human and murine skin, these signatures were reinforced by microbial uptake. In contrast to their adult counterparts or other early life DC subsets, neonatal CD301b$^+$ DC2 highly expressed the retinoic acid-producing enzyme, RALDH2, the deletion of which limited commensal-specific Treg cell generation. Thus, synergistic interactions between bacteria and a specialized DC subset critically support early life tolerance at the cutaneous interface.

eTOC blurb:

Maintenance of cutaneous immune homeostasis, and by extension skin health, requires early life establishment of antigen-specific tolerance to commensal bacteria. Here, Weckel et al. identify that CD301b$^+$ type 2 dendritic cells in neonatal skin critically support this tolerance via retinoic acid-medicated generation of commensal-specific regulatory T cells.

Graphical Abstract

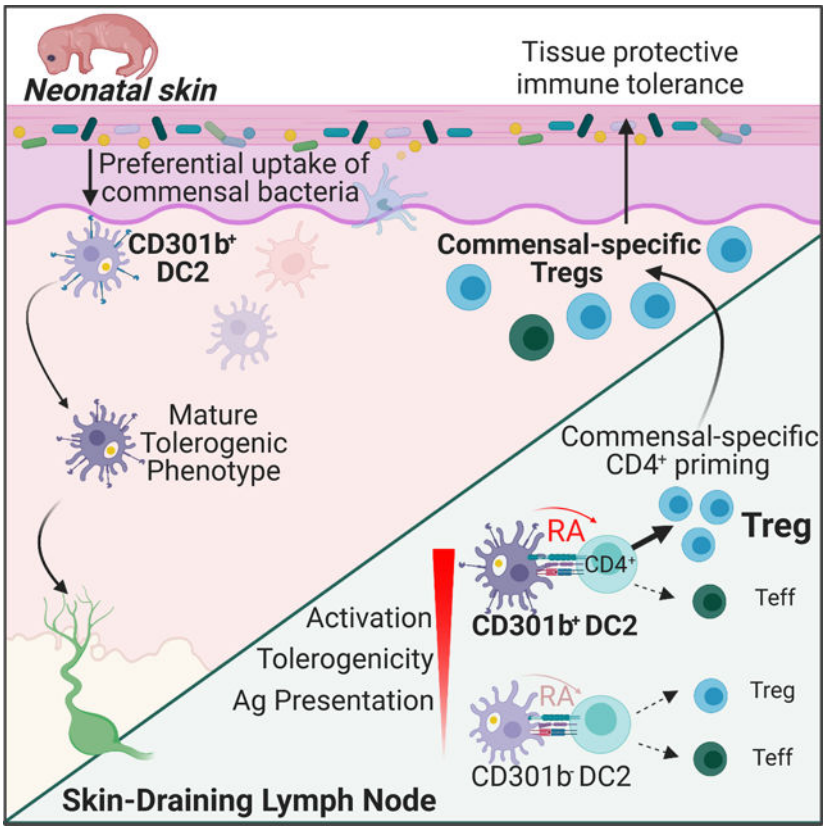

Introduction

Immune tolerance to environmental and commensal-derived antigens fundamentally supports both tissue and systemic immune homeostasis[1]. Early life is a particularly important window for establishing this tolerance, during which tissues are endowed with enriched tolerogenic capacity[2]. However, inherent obstacles to studying neonatal immunity, such as low cell numbers, small organism size, and limited access to human tissues, have contributed to persistent knowledge gaps regarding which cell types and pathways instruct unique early life immunity. Overcoming these challenges is critically important if we hope to intervene early enough to prevent and mitigate the severity of immune-mediated diseases.

Immune tolerance is especially important in the skin, one of the body's most expansive barrier interfaces[3] that is continually exposed to environmental antigens including those from its rich community of bacterial symbionts[4]. A growing body of work demonstrates that commensal bacteria function as key collaborators in many aspects of skin health. They promote physical and antimicrobial barrier integrity, accelerate wound-healing, and tune adaptive immune function[5]. Failure to establish or maintain immune tolerance to skin commensal bacteria can incite or accelerate allergic, autoimmune and other chronic inflammatory skin diseases[6]. Despite this, we still have very limited understanding of the cell types and mechanisms supporting immune tolerance to skin commensal bacteria.

We have shown that early life represents a preferential window for the establishment of immune tolerance to skin commensal bacteria. As has been confirmed more recently in the gut[7–9], this tolerance is marked by generation of commensal-specific regulatory T cells (Treg cells) that limit skin neutrophils upon later life bacterial re-exposure[10]. It remains unclear, however, whether the preferential establishment of immune tolerance in early life reflects a global difference in regulatory capacity across the entire tissue or is directed by a specialized cell subset. The phenotype and function of antigen-presenting cells – more specifically dendritic cells (DCs) – in neonatal skin represents an additional area of limited knowledge. Human fetal skin DCs have broadly been shown to possess tolerogenic function[11], but whether such capacity is enriched in a defined cell subset and the features linked to any such sub-specialization remain unknown. The major mechanisms by which neonatal DCs drive Treg cell generation in the cutaneous periphery and if this changes with age are other outstanding questions.

Here, we took advantage of engineered bacterial strains, in vivo and ex vivo models of murine and human skin colonization, single-cell RNA sequencing and in vitro mechanistic studies to identify a functionally distinct subset of CD301b$^+$ type 2 conventional DC (DC2) in neonatal skin. Enriched for phagocytic, maturation, and tolerance markers, these cells were uniquely equipped to uptake skin bacteria, present their antigens and generate commensal-specific Treg cells. Direct bacterial interaction reinforced these signatures. Although CD301b$^+$ DC2 in adult skin shared similar features, enhanced regulatory capacity of neonatal CD301b$^+$ DC2 was specifically tied to heightened retinoic acid production, implicating this as a neonatally-enriched tolerance mechanism. Collectively, these data suggest that early life tolerance at barrier surfaces does not reflect a broadly-expressed tissue feature, but unique capacities of specialized cell subsets.

Results

CD301b$^+$ DC2 support early life generation of commensal-specific Treg cells

We have demonstrated that neonatal skin colonization by *Staphylococcus epidermidis* expressing the model antigen 2w (*S. epi*-2w) supports an antigen-specific CD4$^+$ compartment enriched in Treg cells[12]. When neonatally-colonized mice are re-challenged with *S. epi*-2w plus skin abrasion they are better protected against skin inflammation than mice previously colonized during adult life[10]. To more precisely define the primary commensal-specific CD4$^+$ response in neonatal versus adult mice, we performed *S. epi*-2w colonization of 7 day-old or 6 week-old mice and measured the 2w-specific and polyclonal CD4$^+$ responses in the skin-draining lymph nodes (SDLN) 13 days later (Fig. 1A). Despite an overall smaller 2w$^+$CD44$^+$CD4$^+$ compartment and slightly lower polyclonal Treg cell frequency in neonatal SDLN (Fig. S1A-B), the percentage of *S. epi*-specific Treg cells was substantially increased following neonatal versus adult colonization (Fig. 1B). This reinforces that early life establishment of long-term tolerance to skin commensal bacteria is closely linked to a Treg-rich primary antigen-specific response following initial *S. epi*-2w colonization.

As dendritic cells shape the quality of CD4$^+$ T cells responses to tissue antigens, we next sought to define the major DC subsets present in neonatal skin and SDLN by performing

cellular indexing of transcriptomes and epitopes by sequencing (CITE-seq) on D10 mice. This confirmed *Epcam*^{hi} Langerhans cells (LC), *Xcr1*^{hi} CD103^{hi} type 1 conventional dendritic cells (DC1) and *Itgam*^{hi} and *Itgam*^{lo} type 2 conventional dendritic cells (CD11b^{hi} and CD11b^{lo} DC2s) as the four main skin DC types, with a separate small cluster of DCs expressing a combination of these markers but primarily defined by their CCR7^{+} status (Figs. 1C-D, S1C). In the SDLN, CD11c$^{lo/hi}$MHCII^{hi} migratory DCs (migDCs) were comprised of the same four DC subsets with different relative prevalence (Figs. S1D-E). The C-type lectin CD301b, encoded by *Mgl2*, marks a portion of DC2 in adult murine skin and other tissues[13–16]. Our CITE-seq data confirmed *Mgl2* and CD301b expression in both CD11b^{hi} and CD11b^{lo} skin DC2 clusters (Fig. 1E), with similar enrichment of CD301b protein but not RNA-level expression in SDLN migDC2 (Fig. S1F). Flow cytometry confirmed CD301b expression by approximately two thirds of neonatal skin DC2s (Figs. 1F, S1G-I).

To systematically assess if a specific DC subset preferentially supports generation of commensal-specific Treg cells, we next used three complementary models to temporarily deplete each of the major skin DC subsets in the neonatal window during *S. epi*-2w colonization (Fig. 1G). As reported in adult mice[17], diphtheria toxin (DT) administration to *Xcr1*^{DTR} mice led to preferential depletion of DC1 in the skin and SDLN (Fig. S1J). Likewise, HuLang^{DTR} mice[18] were a reliable model for LC depletion (Fig. S1K). No model yet exists for transient depletion of all DC2[19], thus we took an alternative strategy of using *Mgl2*^{DTR} mice to achieve robust depletion of CD301b^{+} DC2 in the skin and SDLN, which comparably affected the CD301b^{+} subset of both CD11b^{hi} and CD11b^{lo} DC2 (Fig. S1I and S1L). Examination of 2w^{+}CD44^{+}CD4^{+} T cells in the SDLN at D21 across these models revealed a relative and absolute reduction in *S. epi*-specific Treg cells only in *Mgl2*^{DTR} mice (Fig. 1H-J, S1M). Compared to DT-treated *Mgl2*^{WT} littermates, *Mgl2*^{DTR} mice demonstrated lower numbers of *S. epi*-specific CD4^{+} T cells, driven entirely by a reduction of *S. epi*-specific Treg cells as Foxp3^{-} effector CD4^{+} T (Teff) cells were unchanged (Fig. 1J). Polyclonal Treg percentages were modestly increased in *Mgl2*^{DTR} neonates (Fig. S1N), further emphasizing a specific defect in commensal-specific Treg cells. A similar decrease in the number of *S. epi*-specific Treg cells was seen in *Mgl2*^{cre}*H2ab1*$^{fl/fl}$ (CD301b$^{\Delta MHCII}$) mice[16] (Fig. 1K), which have reduced MHCII expression by CD301b-expressing cells (Fig. S1O), suggesting that antigen-presentation by CD301b^{+} DC2 is specifically needed for optimal Treg generation.

To understand if CD301b^{+} DC2 broadly support generation of Treg cells to skin commensals, we performed depletion experiments in *Mgl2*^{DTR} mice during neonatal colonization with other 2w-expressing commensal *Staphylococcus* species. While the effect on the percentage of Treg cells and total number depended on the strain (Figs. 1L and S1P), the number of commensal-specific Treg cells in the SDLN at D21 was reduced for all strains (Fig. 1L), To see if this tolerogenic function extended to other non-bacterial skin-directed antigens, we topically applied solubilized 2w peptide to DT-treated *Mgl2*^{DTR} mice or control pups. In contrast to commensal-derived 2w antigen, neonatal depletion of CD301b^{+} DC2 in 2w peptide-exposed mice did not lead to an overall reduction in antigen-specific CD4^{+} T cells, rather a modest increase was seen (Fig. S1Q). However, the percentage of Treg cells among these 2w-specific CD4^{+} T cells was significantly reduced, driven by an increase in

antigen-specific CD4$^+$ Teff cells (Figs. 1M and S1Q). Collectively, these results support a critical role for CD301b$^+$ DC2 in neonatal generation of Treg cells, especially those specific for skin commensal bacteria.

Transient neonatal depletion of CD301b$^+$ DC2 limits establishment of long-term tolerance to skin commensal bacteria

To assess the importance of neonatal CD301b$^+$ DC2 in shaping the memory response to *S. epi*-2w, we adapted our previously established re-challenge model (Fig. 2A). In this model, failure to perform neonatal colonization with *S. epi*-2w leads to lack of immune tolerance in adulthood as evidenced by increased skin neutrophils following *S. epi*-2w exposure plus epidermal abrasion[10]. Here we colonized *Mgl2^{WT}* and *Mgl2^{DTR}* littermates with *S. epi*-2w during the first two weeks of life in tandem with DT administration to transiently deplete CD301b$^+$ DC2. Two weeks later, upon recovery of CD301b$^+$ DC2 in *Mgl2^{DTR}* (CD301b$^{\Delta Neo}$) mice (Fig. S2A-B), both groups were re-colonized with *S. epi*-2w in tandem with light tape-stripping (Fig. 2A). Post-challenge, CD301b$^{\Delta Neo}$ mice showed persistently reduced numbers and percentages of *S. epi*-specific Treg cells in the SDLN (Fig. S2C).

CD301b$^{\Delta Neo}$ mice also demonstrated altered skin immune homeostasis, demarcated by an increase in the total number of CD4$^+$ T cells, CD8$^+$ T cells, and dermal γδ cells post-challenge (Fig. 2B). This was also reflected in higher numbers of *S. epi*-specific CD4$^+$ T cells in skin (Fig. 2C), which was driven in large part by increased *S. epi*-specific Teff cells (Fig. 2C). As in the SDLN, the percentage of *S. epi*-specific Treg cells in skin was reduced in CD301b$^{\Delta Neo}$ mice (Fig. 2D), despite equivalent polyclonal Treg percentages (Fig. S2D). Alterations in the commensal-specific response in CD301b$^{\Delta Neo}$ mice were accompanied by increased total numbers of IL-17 producing CD4$^+$ (Th17) T cells (Fig. 2E) and neutrophils (Fig. 2F). These observations closely parallel the response seen in mice that were not colonized neonatally by *S. epi*-2w but only challenged as adults[10], suggesting that CD301b$^+$ DC2 critically support establishment of long-term tolerance to commensal antigens during neonatal colonization.

Neonatal CD301b$^+$ DC2 preferentially uptake skin bacterial antigens for presentation to CD4$^+$ in the SDLN

Given the specific functional role for CD301b$^+$ DC2 in shaping the neonatal CD4$^+$ response to *S. epi*-2w, we next examined their capacity to uptake *S. epi*-expressed antigen, migrate, and present antigen in the SDLN. For this, we first took advantage of *S. epidermidis* expressing a phagolysosome resistant fluorophore, ZsGreen[20] (*S. epi*-ZsGreen) to track its uptake by DCs in neonatally colonized mice (Fig. 3A). By confocal imaging, we visualized bacteria both on the skin surface and dermally in association with hair follicles (Fig. S3A). Flow cytometry of skin revealed preferential *S. epi*-ZsGreen uptake by CD11b^{hi} DC2, both in terms of the percentage of that subset loaded (i.e. *S. epi*-ZsGreen affinity) and the total number of loaded cells, which peaked 16 hours post-colonization (Fig. 3B-C). In the SDLN, migDC numbers increased between 8 and 16 hours post-colonization (Fig. S3B). Among these, CD11b^{hi} DC2 were again overrepresented in terms of *S. epi*-ZsGreen affinity and of the total number of ZsGreen$^+$ cells (Fig. 3D-E), suggesting they transport commensal antigen from skin to the SDLN. Non-DC myeloid populations did

phagocytose *S. epi*-ZsGreen in skin (Fig. S3C), but did not migrate substantially to SDLN post-colonization (Fig. S3B). To understand if preferential uptake by DC2 was conserved across species we colonized the epidermal surface of human neonatal foreskin explants with a physiological amount of *S. epi*-ZsGreen for 4 hours prior to examination of ZsGreen^{+} DCs by flow cytometry (Figs. S3D-E). This revealed that DC2 also constituted the majority of commensal-laden DCs in human skin (Figs. 3F-G).

Next, we examined the capacity of DC2 to present commensal antigen and induce antigen-specific CD4^{+} T cell proliferation. For this, we incubated ovalbumin-expressing *S. epidermidis* (*S. epi*-OVA)[21] overnight with CD11b^{hi} DC2, CD11b^{lo} DC2, DC1 or LC sorted from the migDC population of neonatal SDLN, then co-cultured for 72 hours with cell trace violet (CTV)-labelled OT-II CD4^{+} T cells (Fig. 3H). DCs loaded with OVA, non-OVA-expressing *S. epidermidis* and wells with no DCs were used as controls. In this ex vivo approach, bacterial uptake across DC subsets was somewhat normalized (Fig. S3F), but CD11b^{hi} and LC remained preferentially loaded. Although all DC subsets induced equivalent proliferation of CD8^{+} OT-I T cells (Figs. S3G-H), CD11b^{hi} DC2, followed by LC and CD11b^{lo} DC2, induced more robust CD4^{+} OT-II proliferation in response to OVA and *S. epi*-OVA (Figs. 3I-J, S3I-J).

To determine if CD301b^{+} DC2 are specifically equipped to sample bacterial antigens we re-examined our longitudinal data for in vivo *S. epi*-ZsGreen uptake (Fig. 3A). In both skin DC2 and SDLN migDC2, this revealed a higher *S. epi*-ZsGreen affinity among CD301b^{+} versus CD301b^{-} cells (Fig. 3K-L, S3K-L). Confocal imaging of neonatal skin did not identify differential spatial localization of CD301b^{+} versus CD301b^{-} MHCII^{+} cells (Fig. S3M), and in a separate ex vivo phagocytosis assay CD301b^{+} DC2 sorted from SDLN demonstrated substantially greater uptake of *S. epi*-ZsGreen than CD301b^{-} DC2, when exposed at a multiplicity of infection (MOI) of 10 (Fig. 3M). Thus, in vivo differences in bacterial uptake can at least in part be explained by cell-intrinsic CD301b^{+} DC2 features (Fig. 3M). Using overnight ex vivo incubation of CD301b^{+} or CD301b^{-} DC2 with *S. epi*-ZsGreen at a MOI of 100 to somewhat normalize uptake (Fig. S3N), we then examined their relative capacity to present antigen to CD4^{+} T cells. Increased OT-II proliferation was induced by *S. epi*-OVA-loaded CD301b^{+} versus CD301b^{-} DC2 (Fig. 3N-O), a difference which held also with OVA protein (Fig. S3O). Collectively these results indicate that DC2, specifically those that are CD301b^{+}, are especially equipped for uptake of commensal bacterial in the skin and can present these antigens to CD4^{+} T cells in the SDLN.

CD301b marks a subgroup of activated DC2 enriched for phagocytic, maturation as well as regulatory markers

We next sought to more comprehensively identify defining features of CD301b^{+} versus CD301b^{-} DC2 in the skin and SDLN that might explain their unique role in neonatal generation of commensal-specific Treg cells. CD301b^{+} DC2 in the thymus[22] have been shown to be dependent on type 2 cytokines, as have CD11b^{lo} DC in the skin and SDLN. We therefore examined the fraction of DC2 in neonatal skin and SDLN in *Il14*$^{-/-}$ *Il13*$^{-/-}$, which failed to reveal a dependency on type 2 cytokines (Fig. S4A). Focusing first on skin DC2, we returned to our CITE-seq data from D10 pups, now setting a threshold for *Mgl2*/CD301b

expression to compare CD301b$^+$ versus CD301b$^-$ DC2 cells (Fig. 1E and Fig. S1F). CD301b$^+$ DC2 were enriched for genes and pathways involved in antigen presentation, T cell activation and phagocytosis (Fig. 4A-C, S4B, Table S1 & S2), possibly explaining their higher capacity to uptake and present bacterial antigens (Fig. 3). Spectral flow cytometry showed higher expression of CD80, CD86, CD40, OX-40L but also PD-L1, and PD-L2 on skin CD301b$^+$ DC2, measured either by the percentage of positive cells or their average MFI (Fig. 4D-E), which suggests a mature but also regulatory phenotype. Examination of SDLN CD301b$^+$ versus CD301b$^-$ DC2 revealed transcriptional reduction of phagocytic and other surface receptors as compared to the skin, in tandem with reduced *Mgl2* expression (Fig. S1F). However, SDLN CD301b$^+$ DC2 retained higher surface expression of CD80, CD86, CD40, PD-L1, and PD-L2 compared to CD301b$^-$ DC2 (Fig. S4C-D). They also showed increased RNA-level expression of *Aldh1a2*, which encodes the retinoic acid (RA) producing enzyme RALDH2[23] that supports Treg generation[24], suggesting further consolidation of their regulatory capacity in the SDLN (Table S3).

Based on the in vivo data from *Mgl2*^{DTR} mice and the mature and regulatory phenotype of CD301b$^+$ DC2, we explored these cells' functional ability to support Treg generation ex vivo. CD301b$^+$ and CD301b$^-$ DC2 sorted from the SDLN were incubated overnight with OVA protein then co-cultured with OT-II CD4$^+$ under Treg-inducing conditions with TGF-β and IL-2 (Fig. 4F). This revealed preferential Treg cell generation by CD301b$^+$ versus CD301b$^-$ DC2 (Fig. 4G-H). In contrast, LC generated far fewer Treg cells, despite only a modestly lower capacity to induce CD4$^+$ T cell proliferation (Fig. S4E). Collectively, these data support an intrinsic preferential capacity for antigen uptake by CD301b$^+$ DC2 in skin as well as for antigen presentation and Treg generation in the SDLN.

Uptake of skin commensal bacteria sustains maturation as well as tolerogenic features of CD301b$^+$ DC2

The context of DC antigen encounter, i.e. with or without certain pathogen-associated or damage-associated molecular patterns, influences the secondary and tertiary signals they present in tandem with antigen. These co-stimulatory surface molecules and secreted cytokines, in turn, help dictate the phenotype and function of antigen-specific T cells primed by that DC[25]. Our profiling of neonatal CD301b$^+$ DC2 suggested that homeostatically these cells have a mature but also tolerogenic phenotype, capable of supporting Treg cells. To understand how direct encounter with skin commensal bacteria further impacts this phenotype, we performed single cell RNA sequencing (scRNAseq) on ZsGreen$^+$ and ZsGreen$^-$ DCs sorted from the skin of *S. epi*-ZsGreen colonized neonates (Fig. 5A). This revealed higher expression by ZsGreen$^+$ CD301b$^+$ DC2 of genes known to mediate regulatory DC functions, including Treg generation: *Cd80/Cd86*[26–28], *Fas*[29], *Cd274*[28,30] and *Socs1*[31] (Fig. 5B). The Treg-promoting cytokine, *Il10*[32], was also increased in ZsGreen$^+$ CD301b$^+$ DC2, whereas *Il1b* and *IL-6*, which promote Th17 responses, were expressed more in ZsGreen$^-$ CD301b$^+$ DC2. For most of these markers, protein level increases in ZsGreen$^+$ versus ZsGreen$^-$ skin CD301b$^+$ DC2 from both the skin and SDLN were confirmed by spectral flow cytometry (Fig. 5C, S5A-B). Some additional markers, e.g. OX40L[21], were increased in *S. epi*-ZsGreen$^+$ CD301b$^+$ DC2 at the protein but not mRNA level (Fig. 5C. S5A-B).

Taking advantage of our neonatal foreskin explant system, in which we validated DC2 uptake of *S. epi*-ZsGreen (Fig. 3), we assessed if *S. epidermidis* phagocytosis similarly polarized human skin DCs. After 4 hours of *S. epi*-ZsGreen colonization, ZsGreen$^+$ and ZsGreen$^-$ HLA-DR$^+$ cells were separately sorted and submitted for scRNAseq, after which DC subsets were identified using classical markers (Figs. 5D-E, S5C-D)[33]. Despite the short period post-colonization, *S. epi*-ZsGreen-loaded DC2 demonstrated higher expression of many parallel markers of human regulatory DC function (Fig. 5F)[34].

To assess if CD301b$^+$ DC2 capacity to support Treg cells was sustained upon *S. epidermidis* uptake, we incubated CD301b$^+$ or CD301b$^-$ DC2 overnight with *S. epi*-OVA prior to co-culture with OT-II under Treg-inducing conditions (Fig. 5G). Only CD301b$^+$ DC2 were capable of generating substantial amounts of Treg cells (Figs. 5H-I). In contrast, LC and CD301b$^-$ DC2, despite inducing robust OT-II proliferation (Figs. 3J and 3O), generated fewer *S. epi*-specific Treg cells (Figs. 5H-I). This indicates that the a priori tolerogenic capacity of CD301b$^+$ DC2 is maintained upon uptake of skin commensal bacteria, consistent with in vivo evidence (Figs. 1, S1) that they promote commensal-specific Treg cells.

CD301b$^+$ DC2 exhibit subtle age-dependent changes, with a preserved but reduced capacity for Treg generation in adulthood

Given the preferential generation of commensal-specific Treg cells following neonatal versus adult *S. epi*-2w colonization, we next explored age-dependent features of skin DCs. scRNAseq analysis of neonatal versus adult skin DCs did not show substantial clustering by age, and all major subsets were represented at both time points (Fig 6A). *Mgl2* and CD301b expression were also comparably distributed among DC subsets in adult as compared to neonatal skin (Fig. S6A-B). As in neonates, the proportion of CD301b$^+$ DC2 in adult skin and SDLN was not dependent on type 2 cytokines (Fig. S6C). with the exception of LC, which are known to be prenatally seeded (Fig. 6B). In neonatal dermis, DC1 and CD11b^{lo} DC2 were specifically overrepresented (Fig. 6C). Among SDLN migDCs, the total number of each DC subset trended lower in neonates (Fig. S6D), but DC1 and LC were proportionally enriched in neonates (Fig. S6E).

S. epi-ZsGreen colonization of adult mice, as in neonates, resulted in preferential uptake by skin CD301b$^+$ DC2. However, the overall proportion of bacterially-loaded DCs was higher in adult skin (Fig. 6D). To explore if this corresponded to distinct DC localization, we performed confocal imaging. In spite of gross structural differences associated with skin age, namely decreased hair follicle density and dermal thickness in adulthood, CD301b$^+$ MHCII$^+$ cells in adults were similarly distributed in the upper-middle dermis (Fig S6F). Direct comparison of CD301b$^+$ migDC2 from adult versus neonatal SDLN in our ex vivo phagocytosis assay, revealed lower bacterial uptake by adult cells (Fig 6E). Thus, the etiology of the subtle difference for in vivo uptake remains incompletely understood.

To understand whether CD301b$^+$ DC2 retain the capacity to generate Treg cells to commensal bacteria in adulthood, we colonized the skin of adult *Mgl2*^{DTR} and *Mgl2*^{WT} mice with *S. epi*-2w concurrently with DT treatment. We examined the SDLN 8 days after the last colonization to parallel timing of our neonatal experiments. This confirmed that adult versus neonatal colonization of *Mgl2*^{WT} mice leads to an overall lower percentage

(8 versus 50 percent) of *S. epi*-specific Treg cells (Fig 1J, Fig 6F). Similar to neonates, adult *Mgl2*^{DTR} showed reduced absolute numbers of SDLN *S. epi*-specific CD4$^+$ Treg cells but, in contrast to neonates, also a reduction in *S. epi*-specific CD4$^+$ Teff cells (Fig. 6F). Treg numbers were more impacted, leading to a reduced percentage of *S. epi*-specific Treg cells (Fig. 6F). As in neonates, there were no decreases in polyclonal Treg cells (Fig. S6G). Thus, CD301b$^+$ cells retain some capacity to support commensal-specific Treg cells into adulthood.

We next returned to our scRNAseq data to probe phenotypic differences in skin DC2 by age. In both neonates and adults, CD301b$^+$ versus CD301b$^-$ DC2 were distinguished by similar genes (Fig. 6G-H, Table S4) and gene pathways (Fig. 6I, Table S5). Spectral flow cytometry of adult skin and SDLN largely showed preservation of these CD301b$^+$ versus CD301b$^-$ DC2 differences at the protein level (Fig. 6J). Direct comparison of neonates and adults, however, revealed that transcripts for CD301b$^+$ defining genes and pathways (Fig. 4A-C, S4B, 6G-I; Table S1, S2, S4 & S5) were similarly expressed by skin CD301b$^+$ DC2 irrespective of age (Table S6-S7). Spectral flow cytometry did show higher levels of some surface markers in adult versus neonatal CD301b$^+$ DC2, most notably PDL1 and CD86 (Fig. 6K), with similar but more subtle differences in the SDLN (Fig. S6I).

To directly compare the functional capacity of DC2 from neonatal or adult mice we returned to our ex vivo DC-T cell assay. This showed minimal differences between adult CD301b$^+$ versus CD301b$^-$ DC2 in their ability to induce OT-II proliferation (Fig. 6L) or Treg generation (Fig. 6M). In comparison, neonatal CD301b$^+$ DC2 outperformed adult DCs in both of these areas. Collectively, these data suggest that CD301b$^+$ DC2 retain some ability even in adulthood to support peripheral generation of Treg cells to skin bacteria, but that this capacity is especially enhanced in neonatal DC2. However, our profiling of these two populations at the transcriptional and protein levels did not reveal an obvious mechanistic explanation for this functional result.

RALDH2 activity, enriched in neonatal CD301b$^+$ DC2, supports early life commensal-specific Treg cells

DCs can promote Treg generation via multiple mechanisms[35], but their production of retinoic acid (RA) is strongly linked to this function[24,36], especially in gut-associated lymphoid tissue[36,37] where the RA-precursor, Vitamin A, is in high abundance from dietary sources. Whether there is a role for RA in tolerance at the cutaneous interface, if this tolerance mechanism differs by age and if it can be influenced by commensals, remain unanswered questions. DC production of RA is controlled by retinaldehyde dehydrogenase 2 (RALDH2), encoded by *Aldh1a2*[38].Our scRNAseq identified increased *Aldh1a2* expression in CD11b$^+$ and CD301b$^+$ migDC2 versus other subsets (Fig. 7A & S7A, Table S3). qRT-PCR confirmed a two- to three-fold increase in expression among CD301b$^+$ versus CD301b$^-$ migDC2 in the neonatal SDLN (Figs. 7B and S7B). Parallel analysis of adult SDLN DCs illustrated high *Aldh1a2* expression to be a specific feature of neonatal CD301b$^+$ DC2 versus their adult counterparts (Fig. 7B). Preferential protein-level expression of RALDH in neonatal CD301b$^+$ DC2 was also confirmed via enzymatic assay (Fig. 7C and Fig. S7C). To understand if commensal uptake influences RALDH activity

in CD301b$^+$ DC2, we measured enzyme levels in sorted cells with or without ex vivo phagocytosis of *S. epi*-ZsGreen. RALDH activity was increased in ZsGreen$^+$ cells (Fig. 7D), suggesting that skin commensals can augment this key tolerogenic pathway.

To uncover the in vivo contribution of DC-derived RADLH2 in antigen-specific Treg generation to skin commensal bacteria, we returned to our *S. epi*-2w colonization model, now using *Cd11c^{cre} Aldh1a2$^{fl/fl}$* (DC$^{\Delta Aldh1a2}$) mice, in which qRT-PCR confirmed a 20-fold reduction in DC *Aldh1a2* expression without a corresponding decrease in CD11c$^-$ stromal cells (Fig. S7D). Colonization of DC$^{\Delta Aldh1a2}$ neonates (Fig. 7E) resulted in substantially fewer commensal-specific Treg cells but equivalent numbers of Teff cells in the SDLN at day 21 as compared to *Aldh1a2$^{fl/fl}$* (DC$^{\Delta WT}$) littermates (Fig. 7E-F, S7E). To probe the functional importance of RA production more specifically in CD301b$^+$ DC2 versus other subsets, we isolated CD301b$^+$ and CD301b$^-$ DC2 from the SDLN of neonatal DC$^{\Delta Aldh1a2}$ and DC^{WT} mice and performed DC-T cell co-cultures under Treg-inducing conditions. This revealed a significant contribution of RALDH in Treg cell generation, but not T cell proliferation, by CD301b$^+$ DC2 in response to both soluble and commensal-expressed OVA antigen (Fig. 7G-H, S7F-G). Thus, RA production by neonatal CD301b$^+$ DC2, which is enriched versus other subsets or their adult counterparts, plays a key role in their preferential capacity to support generation of commensal-specific Treg cells.

Discussion

Here we demonstrate CD301b$^+$ DC2 as a critical cell population that supports early life establishment of peripheral tolerance to skin commensal bacteria. This function stems in part from a preferential capacity to sample bacterial antigens, a feature shared with DC2 in human neonatal skin. However, while other DC subsets, such as LC, can also efficiently uptake skin bacteria and present commensal antigens to induce CD4$^+$ T cell proliferation, CD301b$^+$ DC2 demonstrate a unique propensity for Treg generation. Uptake of commensal bacteria by human or murine DC2 sustains key features of their genetic program, namely markers of maturation, antigen presentation, and tolerance. Neonatal and adult murine CD301b$^+$ DC2 share many attributes, but production of RALDH is a distinguishing feature of neonatal CD301b$^+$ DC2 and a key mechanism by which they support Treg generation.

In the intestines, goblet cells have been shown to facilitate uptake of commensal bacteria antigens in the pre-weaning window, forming a cooperative relationship with the DC subsets that present these antigens[39,40]. We demonstrate evolution in skin of parallel but distinct mechanisms to support effective sampling of bacterial antigens during early life, namely a DC population especially equipped with this capacity. This idea that skin DC2 serve a key role in tuning commensal-specific responses is corroborated by prior work showing that they promote IL-17 production by *S. epi*-specific CD8$^+$ T cells[41]. Our imaging did not identify obvious spatial organization of CD301b$^+$ versus CD301b$^-$ DC2, and although subtle spatial sub-localization remains a possibility, our phagocytosis assay and scRNAseq data suggest that preferential phagocytic receptor expression likely drives their efficient uptake of commensal bacteria. In the intestine, CD103$^+$ DCs are recognized as a key DC subset supporting tolerance to commensals via peripheral Treg induction[36]. More recently, Aire-expressing DCs in the intestinal lymph nodes have been identified as an important

cell type contributing to this function[8,42]. This supports the existence of barrier site-specific restriction of this function to distinct DC types.

Work in the thymus has highlighted CD301b as a marker of DC2 possessing enhanced capacity for antigen processing and presentation[22], which parallels our observations in the skin. Additionally, CD301b expression on skin DC2 strongly correlates with their expression of phagocytic receptors and efficient bacterial uptake. Type 2 cytokines have been shown to promote CD301b$^+$ DC2 in the thymus[22] and CD11b^{lo} DC in the skin[43], but we found CD301b$^+$ DC2 cells still present in the skin at equivalent proportions in *Il13*$^{-/-}$*Il4r*$^{-/-}$ mice. Our data, in tandem with this recent work, support a model in which CD301b marks a sub-state of DC2 rather than a separate ontogenetic lineage. However, the specific pathways driving expression of CD301b and associated programs in skin DC2 remain to be determined.

CD301b$^+$ DC2 have been implicated in supporting a range of different T cell responses. They have been studied most in depth in the context of allergic inflammation where they facilitate the differentiation of type 2 helper (Th2) cells[13]. They can also optimize priming of naïve CD4$^+$ T cells in SDLN by detaining these cells near the high endothelial venule for maximal antigen scanning[16]. In other models, they have been shown to support Th17 responses[44,45] and to promote clonal deletion of thymic T cells[22]. This suggests that the function of CD301b$^+$ DC2 is contextual, with our findings reflecting their contributions in a setting of early life tissue homeostasis.

Skin CD301b$^+$ DC2 express both activation markers and molecules associated with regulatory DC function, analogous to tumor-associated ‘mReg’ DC[46] and migratory DCs more generally[47]. Notably, we did not find that DC’s capacity to promote Treg cells was strictly coupled with their ability to induce commensal-specific T cell proliferation. LCs efficiently stimulated CD4$^+$ T cell proliferation but did not generate substantial numbers of Treg cells ex vivo. Likewise, the absence of RALDH in CD301b$^+$ DC2 reduced Treg generation without affecting CD4$^+$ proliferation. Collectively, these studies strengthen a narrative that the capability of DCs to induce Treg cells is not necessarily linked to a state of relative immaturity.

The ability of DCs to support Treg induction and proliferation has been tied to many different pathways and molecules[34], many of which are expressed by CD301b$^+$ DC2. Synergy across multiple mechanisms likely supports Treg generation by these and other tolerogenic DC populations. We were intrigued to find, however, that the RA pathway was specifically enriched among CD301b$^+$ DC2 and increased upon *S. epidermidis* uptake. RA production supports peripheral Treg induction and limits Th1/Th17 differentiation via effects on TGFβ signaling[48,49]. Until now, it has been described primarily in gut-associated lymphoid tissues[37], specifically CD103$^+$ DC[36], and has also been implicated in generation of alpha-4-beta-7 integrin$^+$ gut-homing T cells[50]. RA production and associated Treg-inducting capacity have been hinted at previously in subsets of CD103$^-$ SDLN DC[38]. Our work clearly pinpoints this as a specific feature of CD301b$^+$ DC2 that is preferentially enhanced in early life. Uptake of *S. epidermidis* further increased RALDH expression in these cells, consistent with prior work suggesting that TLR2 and Myd88 signaling can

provide positive feedback loops for RA production[51,52]. Further work is needed however to tease apart interactions between skin commensal bacteria and cutaneous DCs and the extent to which these influence CD301b$^+$ DC function.

While primarily focused on the neonatal window, our work did interrogate age-dependent differences in skin CD301b$^+$ DC2. Reduced commensal-specific Treg cells following either neonatal or adult depletion of CD301b$^+$ cells suggests that some tolerogenic potential extends throughout life. However, whereas neonatal ablation reduced Treg cells from ~50 to 20%, adult ablation reduced Treg cells from ~8 to 4%. This, in tandem with 2–3 time more ex vivo Treg generation by neonatal versus adult CD301b$^+$ DC2, suggests that their Treg-promoting capacity is enhanced early on. While we've identified RALDH expression as a key Treg-promoting pathway that changes in CD301b$^+$ DC2 with age, further work is needed to define other factors that may contribute to their distinct behaviors across the lifespan. Additionally, outside of DC2, there are likely other age-dependent mechanisms contributing to the early window of tolerance in skin that merit deeper study.

Early life microbial interactions impact long-term disease predisposition[53]. While identifying key microbe-derived signals that could be modulated to promote health and prevent disease, our work emphasizes that exposure to the optimal microbiome is insufficient without the properly paired host immune response. In this light, ongoing identification of specific cells and pathways that coordinate tolerogenic capacity of the early life immune system will be foundational to our ability to intervene therapeutically in this window

Limitations of the Study:

The *Mgl2^{DTR}* model depletes DCs as well as CD301b$^+$ macrophages. Our ex vivo experiments with sorted CD301b$^+$ DC2 provide evidence for their particular tolerogenic function and reliance of RA production. However, we cannot exclude that CD301b$^+$ macrophages contribute to the in vivo phenotypes we observed. The focus of this study was to uncover CD301b$^+$ DC2-mediated contributions to early life establishment of tolerance to commensals. Further work is needed to elucidate if neonatal CD301b$^+$ DC2 can support Th2 or Th17 responses in other contexts, as has been demonstrated for their adult counterparts. Likewise, further characterization of human DC2 heterogeneity by age and body site is warranted but challenging to perform especially for early life samples given limited access to those healthy tissues. As bead-enriched OT-II cells were used in our DC-T cell assays we cannot exclude the possibility that a small population of OVA-specific Treg cells present in the original CD4$^+$ pool contributed to our final Treg numbers. Thus, further work is needed to firmly establish whether the preferential Treg-supporting function of CD301b$^+$ DC2 derives entirely from peripheral induction versus preferential expansion. Finally, the fact that some commensal-specific Treg cells remain in CD301b-depleted neonates leaves open the possibility that other cell populations partner with CD301b$^+$ DC2 in their tolerogenic function towards commensals.

RESOURCES AVAILABILITY:

Lead contact

Further information and requests for resources and reagents should be directed to and will be fulfilled by the lead contact, Tiffany Scharschmidt (tiffany.scharschmidt@ucsf.edu).

Material availability

All unique/stable reagents generated in this study are available from the Lead Contact with a completed Materials Transfer Agreement.

Data and code availability

- Schematics were made with Biorender (https://biorender.com). The volcano plots were generated with VolcaNoseR [54]. The panther analysis (http://www.pantherdb.org/) was used with statistical overrepresentation to "GO biological process complete". GraphPad (Prism) 9.3.1 was used. Rstudio v4 was used for scRNAseq analysis.
- The scRNAseq data generated in this study has been deposited to the GEO as indicated in the Key Resources table.
- Codes used for generating figures in Rstudio can be found via the following link: https://github.com/anto-ucsf/CD301b_paper.git and on Zenodo at the following DOI: 10.5281/zenodo.7662384. RDS objects can be downloaded on Mendeley data under the following DOI: 10.17632/j4kt7nmtfm.1
- Any additional information required to reanalyze the data reported in this paper is available from the lead contact upon request.

EXPERIMENTAL MODELS AND SUBJECT DETAILS

Experimental Animals

Wild-type C57BL/6 mice were originally purchased from Jackson Laboratories (Bar Harbor, ME), then bred and maintained in the UCSF specific pathogen-free (SPF) facility on the Parnassus campus for use in experiments. *Xcr1*$^{DTR\text{-}Venus}$ mice were purchased from Jackson[17] and bred in-house. *Mgl2*$^{DTR\text{-}eGFP}$ and *Mgl2*^{Cre}*H2ab1*$^{fl/fl}$ were a gift from Yosuke Kumamoto and Akiko Iwasaki[13,16]. *Cd11c*^{Cre}*Aldh1a2*$^{fl/fl}$ mice[55] were a gift from Randolph Noelle Lab (Dartmouth University), HuLang^{DTR} mice[18] were a gift from Daniel Kaplan (University of Pittsburg). *Il13*$^{-/-}$/*Il4*$^{-/-}$ mice were a gift from Michael Rosenblum (UCSF).

All animals were 7 days to 10 weeks old at the time of experiments. When not otherwise specified, neonate corresponded to D10 to D14 mice, and adult to 6-week to 8-week-old mice. Littermates of the same sex were socially housed under a 12 hours light/dark cycle and randomly assigned to experimental groups whenever possible. Animals of both sexes were used throughout. Animal work was performed in accordance with the NIH Guide for the Care and Use of Laboratory Animals and the guidelines of the Laboratory Animal Resource Center and Institutional Animal Care and Use Committee of the University of California, San Francisco.

Bacterial Strains and Culture Conditions

Staphylococcus epidermidis (*S. epi*) strain Tü3298[56,57] was used in this study and grown in tryptic soy broth at 37°C. Bacterial media was supplemented with 10 μg/mL erythromycin for plasmid selection. In current and published work, *S. epidermidis* has been engineered to express the 2w model antigen linked to the fluorophores mCherry or ZsGreen under control of the *sar* promoter via plasmid pJL74–2W-gpmCherry and pJL74–2W-ZsGreen[12]. The same Tü3298 strain was engineered to express the OVA peptide antigen via modification of the original pJL74–2W-gpmCherry plasmid[21]. In this work, *Staphylococcus hominis* SK119, *Staphylococcus capitis* Scap_DM02D06, *Staphylococcus lugdunensis* Slug_2E06, all provided by Drs. Julie Segre and Heidi Kong, were transformed with the plasmid pJL74–2W-gpmCherry-CAM and cultured in tryptic soy broth supplemented with 15 μg/mL of chloramphenicol at 37°C.

Human Foreskin—Fresh foreskins from elective circumcision of newborn male infants were obtained as deidentified samples under UCSF IRB protocol 10–00944.

METHODS DETAILS

Bacterial Skin Colonization and Light Skin Abrasion Models

S. epi-2w, *S. lugdunensis*-2w, *S. capitis*-2w or *S. hominis*-2w were cultured for 48 hours to achieve high 2w-mCherry expression as measured by flow cytometry, then washed and re-suspended in PBS to obtain 10^8-10^9 colony-forming units (CFUs) at a volume of 100 μL per mouse. For adult mice only, hair was first shaved using electric clippers.

Bacteria were applied via a plastic pipette and a sterile PBS-soaked cotton-tipped swab to the back skin of mice. For neonatal colonization this was performed on days 7, 10, and 13 of life. For adult colonization, this occurred at or just after 6 weeks of age on experimental days D0, D3 and D6. To mimic physiologic exposure of mice to *S. epi*-2w in the context of light skin abrasion during adulthood, back hair was first removed using electric clippers and depilatory cream (Nair™ Hair Remover Body Cream) on day 28 of life, followed by repeated application and removal of adhesive tape on days 28, 31, and 34 (Shurtape HP-500) in tandem with *S. epidermidis* colonization as above. Tissues were harvested on day 37.

Diphtheria Toxin Injection

Mice were intraperitoneally injected with 25 ng/g body weight DT (Sigma, D0564) dissolved in PBS at 2.5 ng/μl concentration.

Soluble 2w-1s peptide primary responses:

Mgl2^{DTR} mice were injected with diphtheria toxin on D6 and D9 per the protocol below. From D7 to D11, 100 μl of 250 μg/mL of 2w-1s peptide in DMSO was applied daily to back skin. SDLN were harvested on D18.

DC-T cell In Vitro Assays

The DC-T cell assay using OVA protein and bacteria was informed by previous work[58], with modifications specific to our model.

DCs: Skin-draining lymph nodes were harvested and processed over sterile 100 μm cell strainers in 1 mL of T cell media (RPMI supplemented with 10% HyClone Characterized Fetal Bovine Serum (FBS), 1% penicillin-streptomycin, 55μM β-mercaptoethanol, 10mM HEPES and 1X GlutaMAX™). Lymph nodes were transferred to digestion media (HBSS, 5% Fetal Calf Serum, 10mM HEPES) containing 500U/mL of Collagenase D (Sigma-Aldrich, Cat 11088866001) and 20 mg/mL of DNAse I, mechanically disrupted and incubated at 37°C for 25 min. Organs were resuspended with a glass pipet and EDTA (10 mM final) was added, and organs were incubated another 5 minutes at 37°C. Tissues were then processed through 100 μm cell strainers, washed and stained. DCs were sorted on a BD FACSAria II using a 100 μm nozzle and sorted into RPMI medium supplemented with 10% FBS. 10,000 DCs were plated in 100 μL of T cell medium with no antibiotics.

Antigens: Soluble antigen: OVA protein was added at 0.5 mg/mL to sorted DCs in T cell medium overnight.

Bacteria: 48 hours cultures of *S. epi*-OVA were spun down, washed and resuspended in T cell medium with no antibiotics. Bacteria were added to sorted DCs to a multiplicity of infection of 100 (10^6 CFU per well), then incubated for 2 hours at 37°C. Gentamycin was added at 25 μg/mL for 2 hours. Cells were washed and incubated overnight at 37°C in T cell medium with antibiotics.

T cells: SDLN and spleen of OTII mice were harvested and processed over sterile wire mesh in 2 mL of complete RPMI media before cell isolation. Adult mice were used unless otherwise specified in legends. Cells were ACK lysed to remove red blood cells and $CD4^+$ T cells were isolated via EasySep™ Mouse $CD4^+$ T Cell Isolation Kit (Catalog No. 19852). Isolation efficiency was verified via flow cytometry. $CD4^+$ T cells were then labeled with the CellTrace™ Violet Cell Proliferation Kit (Invitrogen™, Catalog No. C34557) before co-culturing at 37°C with antigen-pulsed DC at a ratio of 1:10 (100,000 T cells per 10,000 DC). For Treg-inducing conditions, IL-2 (800 U/mL, GoldBio, # 1310-02-100) and TGFβ (40 ng/mL, Peprotech, #100–21C-10UG) were added to the wells. DC and T cells were co-cultured at 37°C for 72 h, then cells were harvested and stained for flow cytometry.

Phagocytosis assay

Cells were processed as for the DC-T cell assay, but the MOI was reduced to 10 (100,000 CFU) and cells were washed, resuspend in distilled water and plated after the gentamycin incubation for CFU enumeration.

Tissue Processing

Lymph nodes and Lymphoid cells: Lymph nodes (skin-draining or mesenteric where specified) were harvested and then processed over sterile wire mesh in 2 mL of complete RPMI media before cell isolation and tetramer staining in PBS.

Lymph nodes and myeloid populations: Harvested lymph nodes were incubated for 20 minutes at 37°C in RPMI with one mL of digestion solution (2 mg/mL collagenase I, 2 mg/mL collagenase IV, 0.1 mg/mL DNase in RPMI with 10mM HEPES, 1% penicillin-

streptomycin and 10% fetal calf serum), resuspended, and further incubated for 15 minutes at 37°C. Cell suspensions were quenched in 9 mL of complete medium and filtered through a 40 μm sterile cell strainer before counting and staining.

Mouse skin processing: Back skin was harvested, lightly defatted, and then washed in PBS by extensive vortexing to reduce free floating bacteria. Skin was then dried and minced with scissors to a fine consistency before tissue digestion in 3 mL complete RPMI (RPMI plus 10% fetal calf serum, 1% penicillin-streptomycin, 55 μM β-mercaptoethanol, 1mM sodium pyruvate, 10mM HEPES and 1X non-essential amino acids) then supplemented with 2 mg/mL collagenase XI, 0.5 mg/mL hyaluronidase, 0.1 mg/mL DNase I. When looking at bacterial uptake in vivo, cytochalasin D (Cayman Chemicals, # 11330) at 2.5 μg/mL was added. Digested skin samples were then incubated, with shaking, at 37°C for 45 minutes before quenching with 15 mL of complete RPMI media and shaking by hand for 30 seconds. Skin cell suspensions were filtered through sterile cell strainers (100 μm followed by 40 μm).

Epidermal preparations: Washed and defatted back skin were floated on a solution of Trypsin 0.5% + 2.5 μg/mL of cytochalasin D for 45 minutes at 37°C. Tissues were transferred to 1 mL of complete RPMI and the epithelial cells were scratched off the tissue. 9 mL of complete RPMI was added and cells filtered through a 40 μm sterile cell strainer.

Human Skin Processing: Neonatal foreskin was finely minced with scissors and incubated in a digestion cocktail containing collagenase IV (3.2 mg/ml, Worthington, LS004186) and DNAse (20 μg/ml, MilliporeSigma, DN251G) diluted in RPMI with 10% fetal bovine serum (FBS), 1% HEPES, 1X non-essential amino acids, 1X Glutamax and 1% penicillin–streptomycin with cytochalasin D 2.5 μg/mL for 2 h at 37 °C. Digests were briefly shaken and passed through a 100 μm strainer to yield a single-cell suspension.

Cell counting: All tissues were re-suspended in 1 mL PBS and 25 μL of cell suspension was mixed with 25 μL of AccuCheck counting beads (Invitrogen,Catalog No. PCB100) for calculating absolute numbers of cells.

Flow Cytometry

Antibody Staining of Myeloid Populations: Cells were stained in PBS for 20 minutes at 4°C with a Live/Dead marker (Ghost Dye Violet510, Tonbo Biosciences, Catalog No. 13–0870-T100). Surface antibodies were added in blocking solution for 30 minutes at 4°C. Cells were washed and fixed in Paraformaldehyde (PFA) for 30 minutes at 4°C.

Antibody Staining of Lymphoid Populations: Cells were stained in blocking solution with a Live/Dead marker (Ghost Dye Violet510, Tonbo Biosciences) for 30 minutes at 4°C. For intracellular staining, cells were fixed and permeabilized using the Foxp3 staining kit (eBioscience, Catalog No. 00–5523-00) buffer for 30 minutes at 4°C then stained in permeabilization buffer for 30 minutes at 4°C.

Cell Re-stimulation for Cytokines: After isolation, skin cells were stimulated with Tonbo kit (1/100 in 1 mL) for 3–6 hours before being processed for staining. A subset of cells was incubated in Brefeldin A to be used as an unstimulated control for gating.

Spectral Flow Cytometry: Cells were incubated with a live-dead dye (ViaDye Red, Cytek Bio) for 20 minutes at 25°C. CCR7 antibody was added for 15 minutes at 37 °C. Surface staining in blocking solution was then added for 30 minutes at 4°C. Cells were fixed with 4% PFA for 15 minutes at 25°C. When populations were bi-modal, geometric MFI was calculated on positive cells, gated as shown in representative histograms.

BandPath and Spectral Flow cytometry: Stained cells were run on a Fortessa (BD Biosciences) or an Aurora (Cytek) in the UCSF Flow Cytometry Core. Flow cytometry data was analyzed using FlowJo software (FlowJo, LLC).

Tetramer Staining and Enrichment: To identify 2w-specific cells, cell suspensions were pelleted and then stained for 1 hour at room temperature (15–25°C), while protected from light, with a 2w1S:I-Ab–streptavidin-phycoerythrin (PE) tetramer at a concentration of 10 nM. Skin was directly stained for other surface and intracellular markers as described above. For LN samples, the tetramer-bound fraction was enriched via an adapted protocol of the EasySep PE Selection Kit II (StemCell Technologies, Inc.) developed by Marc Jenkins' lab. In brief, 6.25 μL of EasySep PE selection cocktail was added to each sample in a total volume of 500 mL and then incubated, while protected from light, at room temperature for 15 minutes. Cells were incubated for an additional 10 minutes after addition of 6.25 μL of EasySep magnetic particles. Finally, cell suspensions were brought up to a total volume of 2.5 mL with PBS and placed into the EasySep magnet for 5 minutes at room temperature. Supernatants (unbound fractions) were poured off into another collection tube. The positively-selected cells (bound fraction) and unbound fraction for each sample were taken for cell counting and staining. For Figure 1L, 1M and S1P and S1Q, SDLN cells were directly stained after the 2w1S:I-Ab–streptavidin-phycoerythrin (PE) tetramer incubation.

Human Foreskin Explant

Explant methodology: Fresh foreskins from elective circumcision of newborn male infants were obtained as deidentified samples, washed in RPMI and cut to generate two explants. Silicone rings were glued to the skin explant using Kwik-Sil silicone glue. Explants were floated in a 12 mm Millicell (Sigma) hanging well on a neutralized solution of 2 mg/mL collagen I in RPMI (Thermo Scientific) at 37°C for 30 minutes until the explant was firmly embedded in a collagen hydrogel. It was then placed in a 12-well plate with the lower chamber filled with RPMI. 5 mL of a 24h culture of *S. epi*-ZsGreen was washed and resuspended in 10 mL of RPMI. 50 μL of this bacterial solution was added to the center of the silicone ring, restraining the contact between bacteria to the stratum corneum. Bacteria were left to interact with the tissue for 30 minutes at 37°C, and the solution of bacteria was then removed to restore an air-skin interface. The explant was left for an additional 4 h at 37°C until tissue processing as above.

Mouse scRNAseq

Live singlet dendritic cells (CD45$^+$ MHCII$^+$ CD11c$^+$) loaded (ZsGreen$^+$) or not loaded (ZsGreen$^-$) from digested back skin or skin draining lymph nodes of control or *S. epi*-ZsGreen colonized D10 neonatal mice and adult (6 week) mice were run on a BD FACSAria II using a 100 μm nozzle and sorted into RPMI medium supplemented with 10% FBS. Cells were sorted from 7–10 pooled mice and different conditions were run on separate lanes of a 10X Chromium chip with 3′ v.2 chemistry (10X Genomics) as per the manufacturer's instructions by the UCSF Institute for Human Genetics Sequencing Core. Libraries were sequenced on an Illumina NovaSeq 6000. FASTQ files were aligned to the mm10 reference genome, and barcode matrices were generated using CellRanger 2.1. For CITE-seq, TotalSeq-A antibodies were added at the same time antibodies for the sort were added. The CITE-seq library was generated according to the manufacturer protocol and sequenced independently.

Downstream data analysis, including clustering, visualizations and exploratory analyses, were performed using Seurat 4.0. Cells with <200 features or more than 5500, or >6% mitochondrial genes were filtered out during preprocessing. Samples sequenced in parallel lanes were merged together for downstream analysis. Principal component analysis (PCA) and uniform manifold approximation and projection (UMAP) were run on the RNA data, and an initial low-resolution clustering was generated using the first 25 principal components. Datasets of figure 1 were clustered based on the RNA transcripts but the protein expression obtained with CITE-seq was used to identify DC clusters using the same defining markers delineated in the flow cytometry gating strategy shown in Figure S1. Datasets of Fig. 5 and Fig.6 used RNA signature based on classical defining markers (*Xcr1* for DC1, *Epcam* Langerhans cells and *Irf4* together with *Itgam* for CD11b^{hi} DC2 and CD11b^{lo} DC2, *Ccr7* for CCR7+ DCs).

Human scRNAseq

Live myeloid cells (CD45$^+$ MHCII$^+$ CD11c$^+$) loaded (ZsGreen$^+$) or not loaded (ZsGreen$^-$) from a neonatal human foreskin explant colonized with *S. epi*-ZsGreen were sorted on a BD FACS Aria II using a 100 μm nozzle into RPMI medium supplemented with 10% FBS. Cells were sorted from 8 explants corresponding to duplicate explants from 4 independent fresh donors (<24h). Downstream processing followed the above mouse scRNAseq protocol, except for the quality control thresholds. Cells below 200 features and above 5000 features or with a percentage of mitochondrial genes above 25% were excluded. Genes used to delineate clusters are shown in Fig. S5. For Fig. 5F, the dendritic cell cluster of Fig. 5E was re-clustered to identify sub-population of dendritic cells.

Quantitative RT-PCR

Indicated populations were sorted into RLT Plus lysis buffer (Qiagen) and stored at −80°C, then processed using Allprep DNA/RNA micro kit (Qiagen) per manufacturer's protocol. For qPCR analyses, RNA was reverse transcribed using SuperScript III cDNA synthesis kit (ThermoFisher) and amplified using Power SYBR Green PCR master mix (ThermoFisher). *Aldh1a2* primers: 5′-GACTTGTAGCAGCTGTCTTCACT-3′, forward, and 5′-TCACCCATTTCTCTCCCATTTCC-3′, reverse. *Rsp17* gene was

used as a housekeeping gene and amplified with the following primers: ATTGAGGTGGATCCCGACAC, forward; TGCCAACTGTAGGCTGAGTG, reverse.

AldeRed Assay

10,000–100,000 sorted cells were plated in a 96 well plate. Staining with AldeRed ALDH detection assay (Sigma) was done following manufacturer's recommendation with minor modifications. To account for the small number of cells, volumes were decreased from the standard protocol recommendations to 100 μL and the reagents AldeRed and DEAB were added at 1 μL per well. Cells were incubated for an hour at 37°C.

Confocal microscopy:

Back skin from neonatal or adult mouse (after shaving) was fixed overnight in periodate-lysin-paraformaldehyde buffer. After two washes in PBS, tissues were incubated overnight in sucrose 30%. Tissues were embedded in optimal cutting temperature compound (OCT) and 20 μm sections were cut on a cryostat. Sections were fixed in blocking buffer (secondary host serum 5%, bovine serum albumin 3% and triton X100 0.3%) for an hour at room temperature. Primary antibodies were incubated in blocking buffer overnight at 4°C, washed at room temperature in PBS and secondary antibodies in blocking buffer were left for up to two hours at room temperature. Tissues were mounted with Prolong Glass Antifade Mountant (Thermofisher). Images were taken with a 20X objective on a CSU-W1 Spinning Disk/High Speed Widefield.

QUANTIFICATION AND STATISTICAL ANALYSIS

Statistical analyses were performed using GraphPad Prism (GraphPad). Data in Figs 3C, 3E, 3L, S3B, S3C and S3L are shown as SEM. For flow cytometry and CFU counts, statistical analyses were performed with Mann-Whitney U (MWU) test for com parison of two groups. One-way and two-way ANOVA were used for comparisons of more than one group, as indicated in the figures. Šídák's multiple comparisons test were used for two-way ANOVA. Nonparametric tests were used as the small sample sizes in our study did not allow us to assume a normal distribution.

Supplementary Material

Refer to Web version on PubMed Central for supplementary material.

Acknowledgements:

We thank Dr. James Moon for 2w tetramer reagents and expertise, and Drs. Yasmine Belkaid, James Gardner, Margaret Lowe, Clifford Lowell, Michael Rosenblum, and Ari Molofsky for helpful discussions. We thank Michelle Chu for help in cloning the *S. epi*-OVA strain, Yongmei Hu for mouse husbandry, and Sepideh Nozzari for genotyping. We appreciate sharing of mouse strains by Drs. Daniel Kaplan, Max Krummel, Randolph Noelle, and Michael Rosenblum and of bacterial strains by Drs. Julia Segre and Heidi Kong. We acknowledge UCSF's PFCC (RRID:SCR_018206) for assistance in flow cytometry and cell sorting, supported by NIH grants P30 DK063720 and 1S10OD021822-01. We acknowledge the UCSF Genomics CoLab in supporting generation of CITE-seq and scRNAseq data. Microscopy was performed at the Nikon Imaging Center at UCSF. M.O.D. is supported by NIAMS K99AR079554. This work was primarily funded by T.C.S. grants NIAMS R01AR080034, NIAID DP2AI144968, and Burroughs Wellcome Fund CAMS-1015631.

References

1. Gensollen T, Iyer SS, Kasper DL, and Blumberg RS (2016). How colonization by microbiota in early life shapes the immune system. Science (1979) 352, 539–544. 10.1126/SCIENCE.AAD9378.
2. Skevaki C, and Thornton CA (2020). Editorial: Early Life Origins of Immune-Mediated Disease. Front Immunol 11, 2050. 10.3389/FIMMU.2020.02050/BIBTEX. [PubMed: 33013866]
3. Gallo RL (2017). Human Skin Is the Largest Epithelial Surface for Interaction with Microbes. J Invest Dermatol 137, 1213–1214. 10.1016/j.jid.2016.11.045. [PubMed: 28395897]
4. Byrd AL, Belkaid Y, and Segre JA (2018). The human skin microbiome. Nat Rev Microbiol 16, 143–155. 10.1038/nrmicro.2017.157. [PubMed: 29332945]
5. Harris-Tryon TA, and Grice EA (2022). Microbiota and maintenance of skin barrier function. Science (1979) 376, 940–945. 10.1126/SCIENCE.ABO0693.
6. Carmona-Cruz S, Orozco-Covarrubias L, and Sáez-de-Ocariz M. (2022). The Human Skin Microbiome in Selected Cutaneous Diseases. Front Cell Infect Microbiol 12, 145. 10.3389/fcimb.2022.834135.
7. Zegarra-Ruiz DF, Kim D. v., Norwood K, Kim M, Wu W-JH, Saldana-Morales FB, Hill AA, Majumdar S, Orozco S, Bell R, et al. (2021). Thymic development of gut-microbiota-specific T cells. Nature 2021 594:7863 594, 413–417. 10.1038/s41586021-03531-1.
8. Akagbosu B, Tayyebi Z, Shibu G, Iza YAP, Deep D, Parisotto YF, Pasolli HA, Elmentaite R, Knott M, Hemmers S, et al. (2022). A novel lineage of RORγt+Aire+ antigen presenting cells promotes peripheral generation of intestinal regulatory T cells and tolerance during early life. bioRxiv, 2022.02.26.481148. 10.1101/2022.02.26.481148.
9. Knoop KA, Gustafsson JK, McDonald KG, Kulkarni DH, Coughlin PE, McCrate S, Kim D, Hsieh CS, Hogan SP, Elson CO, et al. (2017). Microbial antigen encounter during a preweaning interval is critical for tolerance to gut bacteria. Sci Immunol 2. 10.1126/SCIIMMUNOL.AAO1314.
10. Scharschmidt TC, Vasquez KS, Truong H-A, Gearty S. v, Pauli ML, Nosbaum A, Gratz IK, Otto M, Moon JJ, Liese J, et al. (2015). A wave of regulatory T cells into neonatal skin mediates tolerance to commensal microbes. Immunity 43.
11. McGovern N, Shin A, Low G, Low D, Duan K, Yao LJ, Msallam R, Low I, Shadan NB, Sumatoh HR, et al. (2017). Human fetal dendritic cells promote prenatal T-cell immune suppression through arginase-2. Nature 546, 662–666. 10.1038/nature22795. [PubMed: 28614294]
12. Leech JM, Dhariwala MO, Lowe MM, Chu K, Merana GR, Cornuot C, Weckel A, Ma JM, Leitner EG, Gonzalez JR, et al. (2019). Toxin-Triggered Interleukin-1 Receptor Signaling Enables Early-Life Discrimination of Pathogenic versus Commensal Skin Bacteria. Cell Host Microbe 26, 795–809.e5. 10.1016/j.chom.2019.10.007. [PubMed: 31784259]
13. Kumamoto Y, Linehan M, Weinstein JS, Laidlaw BJ, Craft JE, and Iwasaki A. (2013). CD301b^{+} dermal dendritic cells drive T helper 2 cell-mediated immunity. Immunity 39, 733–743. 10.1016/j.immuni.2013.08.029. [PubMed: 24076051]
14. Linehan JL, Dileepan T, Kashem SW, Kaplan DH, Cleary P, and Jenkins MK (2015). Generation of Th17 cells in response to intranasal infection requires TGF-β1 from dendritic cells and IL-6 from CD301b+ dendritic cells. Proc Natl Acad Sci U S A 112, 12782–12787. 10.1073/PNAS.1513532112. [PubMed: 26417101]
15. Shin H, Kumamoto Y, Gopinath S, and Iwasaki A. (2016). CD301b+ dendritic cells stimulate tissue-resident memory CD8+ T cells to protect against genital HSV-2. Nat Commun 7, 1–10. 10.1038/ncomms13346.
16. Tatsumi N, Codrington AL, El-Fenej J, Phondge V, and Kumamoto Y. (2021). Effective CD4 T cell priming requires repertoire scanning by CD301b+ migratory cDC2 cells upon lymph node entry. Sci Immunol 6. 10.1126/sciimmunol.abg0336.
17. Yamazaki C, Sugiyama M, Ohta T, Hemmi H, Hamada E, Sasaki I, Fukuda Y, Yano T, Nobuoka M, Hirashima T, et al. (2013). Critical Roles of a Dendritic Cell Subset Expressing a Chemokine Receptor, XCR1. The Journal of Immunology 190, 6071–6082. 10.4049/JIMMUNOL.1202798. [PubMed: 23670193]

18. Bobr A, Olvera-Gomez I, Igyarto BZ, Haley KM, Hogquist KA, and Kaplan DH (2010). Acute ablation of Langerhans cells enhances skin immune responses. J Immunol 185, 4724–4728. 10.4049/jimmunol.1001802. [PubMed: 20855870]
19. Loschko J, Rieke GJ, Schreiber HA, Meredith MM, Yao KH, Guermonprez P, and Nussenzweig MC (2016). Inducible targeting of cDCs and their subsets in vivo. J Immunol Methods 434, 32–38. 10.1016/J.JIM.2016.04.004. [PubMed: 27073171]
20. Matz M. v., Fradkov AF, Labas YA, Savitsky AP, Zaraisky AG, Markelov ML, and Lukyanov SA (1999). Fluorescent proteins from nonbioluminescent Anthozoa species. Nature Biotechnology 1999 17:10 17, 969–973. 10.1038/13657.
21. Merana GR, Dwyer LR, Dhariwala MO, Weckel A, Gonzalez JR, Okoro JN, Cohen JN, Tamaki CM, Han J, Tasoff P, et al. (2022). Intestinal inflammation alters the antigen-specific immune response to a skin commensal. Cell Rep 39, 110891. 10.1016/J.CELREP.2022.110891.
22. Breed ER, Vobořil M, Ashby KM, Martinez RJ, Qian L, Wang H, Salgado OC, O'Connor CH, and Hogquist KA (2022). Type 2 cytokines in the thymus activate Sirpα+ dendritic cells to promote clonal deletion. Nature Immunology 2022, 1–10. 10.1038/s41590-022-01218-x.
23. Larange A, and Cheroutre H. (2016). Retinoic Acid and Retinoic Acid Receptors as Pleiotropic Modulators of the Immune System. Annu Rev Immunol 34, 369–394. 10.1146/ANNUREV-IMMUNOL-041015-055427. [PubMed: 27168242]
24. Mucida D, Pino-Lagos K, Kim G, Nowak E, Benson MJ, Kronenberg M, Noelle RJ, and Cheroutre H. (2009). Retinoic Acid Can Directly Promote TGF-β-Mediated Foxp3+ Treg Cell Conversion of Naive T Cells. Immunity 30, 471–472. 10.1016/J.IMMUNI.2009.03.008. [PubMed: 19371709]
25. Gool SW, Vandenberghe P, Boer M. de, and Ceuppens JL (1996). CD80, CD86 and CD40 Provide Accessory Signals in a Multiple-Step T-Cell Activation Model. Immunol Rev 153, 47–83. 10.1111/j.1600-065X.1996.tb00920.x. [PubMed: 9010719]
26. Bar-On L, Birnberg T, Kim K, and Jung S. (2011). Dendritic cell-restricted CD80/86 deficiency results in peripheral regulatory T-cell reduction but is not associated with lymphocyte hyperactivation. Eur J Immunol 41, 291–298. 10.1002/EJI.201041169. [PubMed: 21267999]
27. Salomon B, Lenschow DJ, Rhee L, Ashourian N, Singh B, Sharpe A, and Bluestone JA (2000). B7/CD28 Costimulation Is Essential for the Homeostasis of the CD4+CD25+ Immunoregulatory T Cells that Control Autoimmune Diabetes. Immunity 12, 431–440. 10.1016/S1074-7613(00)80195-8. [PubMed: 10795741]
28. Francisco LM, Salinas VH, Brown KE, Vanguri VK, Freeman GJ, Kuchroo VK, and Sharpe AH (2009). PD-L1 regulates the development, maintenance, and function of induced regulatory T cells. Journal of Experimental Medicine 206, 3015–3029. 10.1084/JEM.20090847. [PubMed: 20008522]
29. Qian C, Qian L, Yu Y, An H, Guo Z, Han Y, Chen Y, Bai Y, Wang Q, and Cao X. (2013). Fas Signal Promotes the Immunosuppressive Function of Regulatory Dendritic Cells via the ERK/β-Catenin Pathway *. Journal of Biological Chemistry 288, 27825–27835. 10.1074/JBC.M112.425751. [PubMed: 23943615]
30. Vogel A, Martin K, Soukup K, Halfmann A, Kerndl M, Brunner JS, Hofmann M, Oberbichler L, Korosec A, Kuttke M, et al. (2022). JAK1 signaling in dendritic cells promotes peripheral tolerance in autoimmunity through PD-L1-mediated regulatory T cell induction. Cell Rep 38, 110420. 10.1016/J.CELREP.2022.110420.
31. Fu H, Song S, Liu F, Ni Z, Tang Y, Shen X, Xiao L, Ding G, and Wang Q. (2009). Dendritic cells transduced with SOCS1 gene exhibit regulatory DC properties and prolong allograft survival. Cell Mol Immunol 6, 87–95. 10.1038/cmi.2009.12. [PubMed: 19403057]
32. Chaudhry A, Samstein RM, Treuting P, Liang Y, Pils MC, Heinrich J-M, Jack RS, Wunderlich FT, Brüning JC, Müller W, et al. (2011). Interleukin-10 signaling in regulatory T cells is required for suppression of Th17 cell-mediated inflammation. Immunity 34, 566. 10.1016/J.IMMUNI.2011.03.018. [PubMed: 21511185]
33. Haniffa M, Gunawan M, and Jardine L. (2015). Human skin dendritic cells in health and disease. J Dermatol Sci 77, 85. 10.1016/J.JDERMSCI.2014.08.012. [PubMed: 25301671]
34. Domogalla MP, Rostan P. v, Raker VK, and Steinbrink K. (2017). Tolerance through Education: How Tolerogenic Dendritic Cells Shape Immunity. Front Immunol 8. 10.3389/fimmu.2017.01764.

35. Steinman RM, Hawiger D, and Nussenzweig MC (2003). Tolerogenic Dendritic Cells*. 10.1146/annurev.immunol.21.120601.141040 21, 685–711. 10.1146/ANNUREV.IMMUNOL.21.120601.141040.

36. Coombes JL, Siddiqui KRR, Arancibia-Carcamo C. v, Hall J, Sun CM, Belkaid Y, and Powrie F. (2007). A functionally specialized population of mucosal CD103+ DCs induces Foxp3+ regulatory T cells via a TGF- and retinoic acid dependent mechanism. J Exp Med 204, 1757–1764. 10.1093/nar/29.9.e45. [PubMed: 17620361]

37. Sun C-MM, Hall JA, Blank RB, Bouladoux N, Oukka M, Mora JR, and Belkaid Y. (2007). Small intestine lamina propria dendritic cells promote de novo generation of Foxp3 T reg cells via retinoic acid. Journal of Experimental Medicine 204, 1775–1785. 10.1084/jem.20070602. [PubMed: 17620362]

38. Guilliams M, Crozat K, Henri S, Tamoutounour S, Grenot P, Devilard E, de Bovis B, Alexopoulou L, Dalod M, and Malissen B. (2010). Skin-draining lymph nodes contain dermis-derived CD103− dendritic cells that constitutively produce retinoic acid and induce Foxp3+ regulatory T cells. Blood 115, 1958–1968. 10.1182/blood-2009-09-245274. [PubMed: 20068222]

39. Rios D, Wood MB, Li J, Chassaing B, Gewirtz AT, and Williams IR (2015). Antigen sampling by intestinal M cells is the principal pathway initiating mucosal IgA production to commensal enteric bacteria. Mucosal Immunology 2016 9:4 9, 907–916. 10.1038/mi.2015.121.

40. Kulkarni DH, Gustafsson JK, Knoop KA, McDonald KG, Bidani SS, Davis JE, Floyd AN, Hogan SP, Hsieh C-S, and Newberry RD (2019). Goblet cell associated antigen passages support the induction and maintenance of oral tolerance. Mucosal Immunology 2019 13:2 13, 271–282. 10.1038/s41385-019-0240-7.

41. Naik S, Bouladoux N, Linehan JL, Han S-J, Harrison OJ, Wilhelm C, Conlan S, Himmelfarb S, Byrd AL, Deming C, et al. (2015). Commensal–dendritic-cell interaction specifies a unique protective skin immune signature. Nature 520, 104–108. 10.1038/nature14052. [PubMed: 25539086]

42. Wang J, Lareau CA, Bautista JL, Gupta AR, Sandor K, Germino J, Yin Y, Arvedson MP, Reeder GC, Cramer NT, et al. (2021). Single-cell multiomics defines tolerogenic extrathymic Aire-expressing populations with unique homology to thymic epithelium. Sci Immunol 6. 10.1126/SCIIMMUNOL.ABL5053.

43. Mayer JU, Hilligan KL, Chandler JS, Eccles DA, Old SI, Domingues RG, Yang J, Webb GR, Munoz-Erazo L, Hyde EJ, et al. (2021). Homeostatic IL-13 in healthy skin directs dendritic cell differentiation to promote TH2 and inhibit TH17 cell polarization. Nature Immunology 2021 22:12 22, 1538–1550. 10.1038/s41590-021-01067-0. [PubMed: 34795444]

44. Linehan JL, Dileepan T, Kashem SW, Kaplan DH, Cleary P, and Jenkins MK (2015). Generation of Th17 cells in response to intranasal infection requires TGF-β1 from dendritic cells and IL-6 from CD301b+ dendritic cells. Proc Natl Acad Sci U S A 112, 12782–12787. 10.1073/PNAS.1513532112. [PubMed: 26417101]

45. Kim TG, Kim SH, Park J, Choi W, Sohn M, Na HY, Lee M, Lee JW, Kim SM, Kim DY, et al. (2018). Skin-Specific CD301b+ Dermal Dendritic Cells Drive IL-17−Mediated Psoriasis-Like Immune Response in Mice. Journal of Investigative Dermatology 138, 844–853. 10.1016/J.JID.2017.11.003. [PubMed: 29138056]

46. Maier B, Leader AM, Chen ST, Tung N, Chang C, LeBerichel J, Chudnovskiy A, Maskey S, Walker L, Finnigan JP, et al. (2020). A conserved dendritic-cell regulatory program limits antitumour immunity. Nature 580, 257–262. 10.1038/s41586-020-2134-y. [PubMed: 32269339]

47. Nirschl CJ, Suárez-Fariñas M, Izar B, Prakadan S, Dannenfelser R, Tirosh I, Liu Y, Zhu Q, Devi KSP, Carroll SL, et al. (2017). IFNγ-Dependent Tissue-Immune Homeostasis Is Co-opted in the Tumor Microenvironment. Cell 170, 127–141.e15. 10.1016/j.cell.2017.06.016. [PubMed: 28666115]

48. Mucida D, Park Y, Kim G, Turovskaya O, Scott I, Kronenberg M, and Cheroutre H. (2007). Reciprocal TH17 and Regulatory T Cell Differentiation Mediated by Retinoic Acid. Science (1979) 317, 256–260. 10.1126/SCIENCE.1145697.

49. Xiao S, Jin H, Korn T, Liu SM, Oukka M, Lim B, and Kuchroo VK (2008). Retinoic Acid Increases Foxp3+ Regulatory T Cells and Inhibits Development of Th17 Cells by Enhancing

TGF-β-Driven Smad3 Signaling and Inhibiting IL-6 and IL-23 Receptor Expression. The Journal of Immunology 181, 2277–2284. 10.4049/JIMMUNOL.181.4.2277. [PubMed: 18684916]

50. Benson MJ, Pino-Lagos K, Rosemblatt M, and Noelle RJ (2007). All-trans retinoic acid mediates enhanced T reg cell growth, differentiation, and gut homing in the face of high levels of co-stimulation. Journal of Experimental Medicine 204, 1765–1774. 10.1084/JEM.20070719. [PubMed: 17620363]
51. Villablanca EJ, Wang S, Calisto J. de, Gomes DCO, Kane MA, Napoli JL, Blaner WS, Kagechika H, Blomhoff R, Rosemblatt M, et al. (2011). MyD88 and Retinoic Acid Signaling Pathways Interact to Modulate Gastrointestinal Activities of Dendritic Cells. Gastroenterology 141, 176–185. 10.1053/J.GASTRO.2011.04.010. [PubMed: 21596042]
52. Wang S, Villablanca EJ, Calisto J. de, Gomes DCO, Nguyen DD, Mizoguchi E, Kagan JC, Reinecker H-C, Hacohen N, Nagler C, et al. (2011). MyD88-Dependent TLR1/2 Signals Educate Dendritic Cells with Gut-Specific Imprinting Properties. The Journal of Immunology 187, 141–150. 10.4049/JIMMUNOL.1003740. [PubMed: 21646294]
53. Brodin P. (2022). Immune-microbe interactions early in life: A determinant of health and disease long term. Science (1979) 376, 945–950. 10.1126/SCIENCE.ABK2189.
54. Goedhart J, and Luijsterburg MS (2020). VolcaNoseR is a web app for creating, exploring, labeling and sharing volcano plots. Sci Rep 10, 20560. 10.1038/s41598-020-76603-3.
55. Ji SJ, Zhuang BQ, Falco C, Schneider A, Schuster-Gossler K, Gossler A, and Sockanathan S. (2006). Mesodermal and neuronal retinoids regulate the induction and maintenance of limb innervating spinal motor neurons. Dev Biol 297, 249–261. 10.1016/J.YDBIO.2006.05.015. [PubMed: 16781703]
56. Allgaier H, Jung G, Werner RG, Schneider U, and Zähner H. (1986). Epidermin: sequencing of a heterodetic tetracyclic 21-peptide amide antibiotic. European journal of biochemistry / FEBS 160, 9–22.
57. Augustin J., and Gotz F. (1990). Transformation of Staphylococcus epidermidis and other staphylococcal species with plasmid DNA by electroporation. FEMS Microbiol Lett 54, 203–207. [PubMed: 2182373]
58. Brown CC, Gudjonson H, Pritykin Y, Deep D, Lavallée V-P, Mendoza A, Fromme R, Mazutis L, Ariyan C, Leslie C, et al. (2019). Transcriptional Basis of Mouse and Human Dendritic Cell Heterogeneity. Cell 179, 846–863.e24. 10.1016/j.cell.2019.09.035. [PubMed: 31668803]

Highlights:

- Neonatal skin CD301b$^+$ DC2 efficiently capture, traffic & present commensal antigens
- CD301b$^+$ DC2 have a mature tolerogenic phenotype, accentuated by commensal uptake
- Neonatal Treg generation by CD301b$^+$ DC2 supports commensal-specific tolerance
- CD301b$^+$ DC2 RALDH expression is higher neonatally, promoting their Treg generation

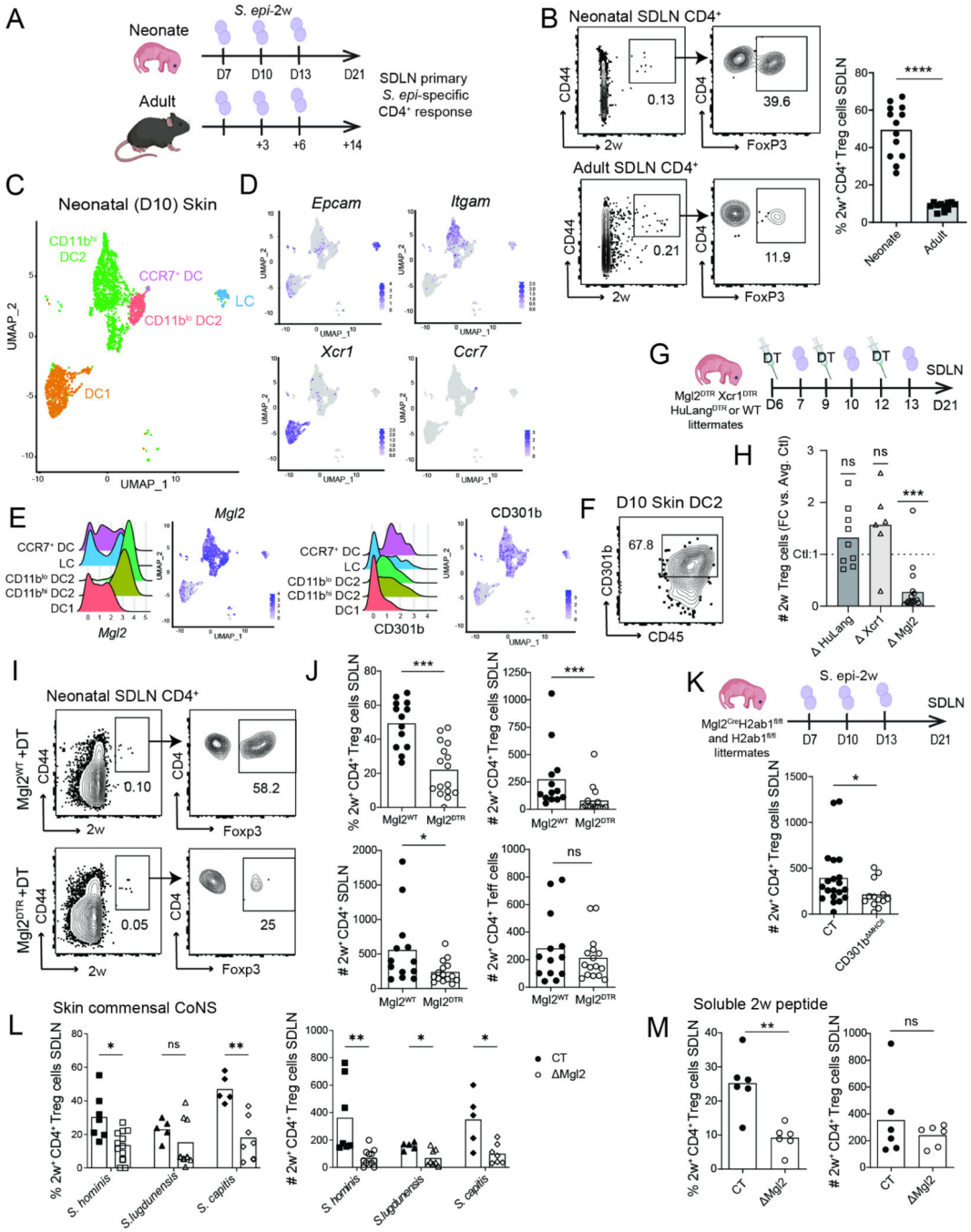

Figure 1: CD301b^{+} DC2 are required for early life generation of skin commensal-specific Treg cells

(A) Adult and neonatal mice were colonized with *S. epi*-2w 3 times every 3 days then harvested a week later; (B) Gating of 2w^{+}CD44^{+}CD4^{+} T cells (2w^{+} CD4^{+} T cells) and 2w^{+}CD44^{+}FoxP3^{+}CD4^{+} Treg (2w^{+} Treg cells) (left), and percentage of 2w^{+} Treg cells in skin draining lymph nodes (SDLN) (pre-gating: live Lin(CD11b, CD11c, F4/80, B220)$^{-}$TCRβ^{+}CD4^{+}). Data from 2–3 independent experiments. (C) UMAP and (D) major defining genes of DC neonatal skin DCs subsets by CITE-seq. (E) Expression of *Mgl2* (left) and its protein CD301b (right). (F) Gating for CD301b on D11 skin DC2 (pre-gating:

live $CD45^+CD11c^+MHCII^+CD103^-EpCam^-$). (G) Experimental setup for (H-J). (H) Fold-change vs. littermate controls of total $2w^+$ Treg cells in the indicated mouse models. One sample Wilcoxon test to hypothetical value of 1. Data from 2–3 independent experiments. (I) Gating of $2w^+$ Treg cells and (J) Percentage and total numbers of $2w^+$ Treg cells and $2w^+CD44^+CD4FoxP3^-CD4^+$ Teff cells ($2w^+$ Teff cells) in the SDLN of DT-treated $Mgl2^{WT}$ and $Mgl2^{DTR}$ mice at D21. (K) Experimental set-up and quantification of $2w^+$ Treg cells in SDLN in of $Mgl2^{cre}H2ab1^{fl/fl}$ and $H2ab1^{fl/fl}$ littermates. Pooled data from 3 independent experiments. (L) Percentage (left) and total numbers (right) of $2w^+$ Treg cells in the SDLN of D21 mice neonatally colonized by 2w-expressing coagulase negative staphylococci (CoNS). Pooled data from two independent experiments. Two-way ANOVA. (M) Percentage (left) and total numbers (right) of $2w^+$ Treg cells in SDLN of D21 mice topically treated with solubilized 2w peptide. One representative experiment of two is shown. Dots represent individual mice. Unless specified Mann-Whitney test was used with *$p < 0.05$, **$p < 0.01$, ***$p < 0.001$, ****$p<0.0001$, ns = not significant.

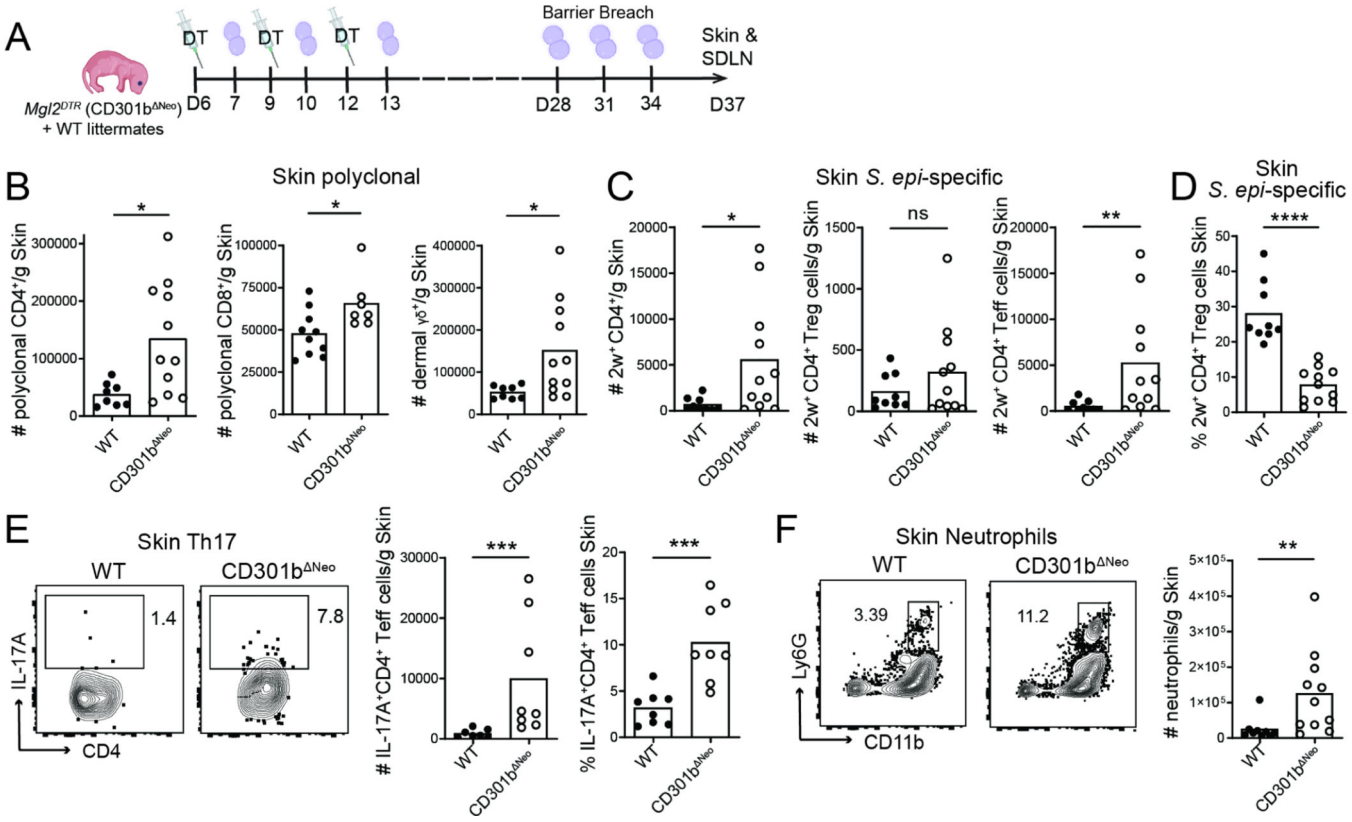

Figure 2: Neonatal CD301b$^+$ DC2 are required for establishment of long-term tolerance to skin commensals

(A) Mice were treated neonatally with DT and *S. epi*-2w (as in Fig. 1G), aged out for 2 weeks, then re-colonized concurrent with skin barrier disruption. (B) Total numbers of polyclonal CD4$^+$ (left), CD8$^+$ (center) and γδ (right) T cells per gram of skin. (C) Total numbers of 2w$^+$ CD4$^+$ (left), 2w$^+$ Treg cells (center) and 2w$^+$ Teff cells (right) per gram of skin. (D) Percentage of 2w$^+$ Treg cells in skin. (E) Representative gating (pre-gating: live TCRβ$^+$CD4$^+$FoxP3$^-$) (left), total numbers per gram of skin (center), and percentage (right) of skin IL-17A$^+$ CD4$^+$ Teff cells. (F) Representative gating (pre-gating: live CD45$^+$CD3$^-$) (left) and total numbers (right) of neutrophils per gram of skin. (A-F) 2–3 independent experiments pooled. Dots represent individual mice. Mann-Whitney test was used with *p < 0.05, **p < 0.01, ***p < 0.001, ****p<0.0001, ns = not significant.

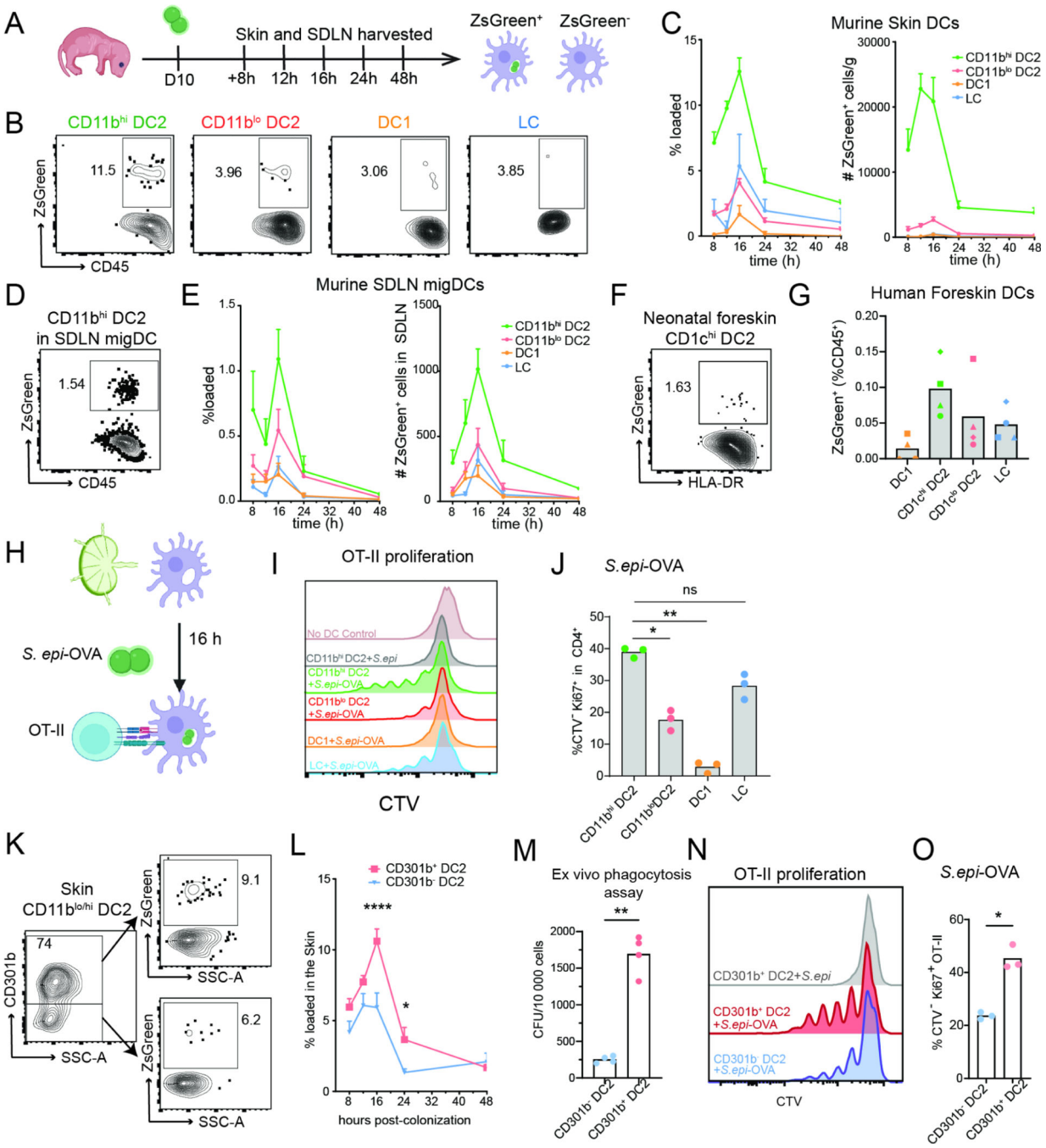

Figure 3: CD301b^{+} DC2s preferentially take up commensal bacteria in mouse and human neonatal skin to present these antigens in the SDLN

(A) Schematic related to B-E and K-L. Neonatal mice were colonized with *S. epi*-ZsGreen, before skin and SDLN were harvested at multiple time points to detect ZsGreen^{+} *S. epi*-loaded DCs. (B) Gating of ZsGreen^{+} cells among skin DC subsets 16h after colonization (pre-gating: per Fig. S1G). (C) Time course of bacterial uptake by skin DCs. Percentage (left) and total number per gram of skin (right) of loaded cells (ZsGreen^{+}) in each population. (D) Sample gating of ZsGreen^{+} CD11b^{hi} migDC2 in the SDLN 16h post-colonization (pre-gating: per Fig. S1H). (E) Time course of ZsGreen^{+} loaded migDC subsets

in SDLN as a percentage of each population (left) or total number (right). (F) Sample gating and (G) enumeration of bacterial uptake by DC subsets in human neonatal foreskin explants 4h after ex vivo *S. epi*-ZsGreen colonization (pre-gating: per Fig. S3E). Each dot represents a separate human donor. 2 independent experiments pooled. (H) Schematic of the approach in I-J and N-O. DC-T cell assay with migDC subtypes sorted from neonatal SDLN, *S. epi*-OVA and CTV-labelled OT-II $CD4^+$ T cells. (I) and (N) Histograms of OT-II CTV dilution, which is quantified in (J) and (O). Each dot in J and O represents a biological replicate pooled from 3 independent experiments. (K) Sample gating and (L) time course of commensal uptake by $CD301b^+$ vs. $CD301b^-$ DC2 in neonatal skin. (M) *S. epidermidis* uptake by neonatal $CD301b^+$ vs. $CD301b^-$ SDLN migDC2 in ex vivo phagocytosis assay. (C, E and L) SEM of 4 mice per time point. (J) One-way ANOVA with Dunnett's post-test. (M, O) Student's paired t-test. * $p < 0.05$, ** $p < 0.01$, *** $p < 0.001$, **** $p < 0.0001$

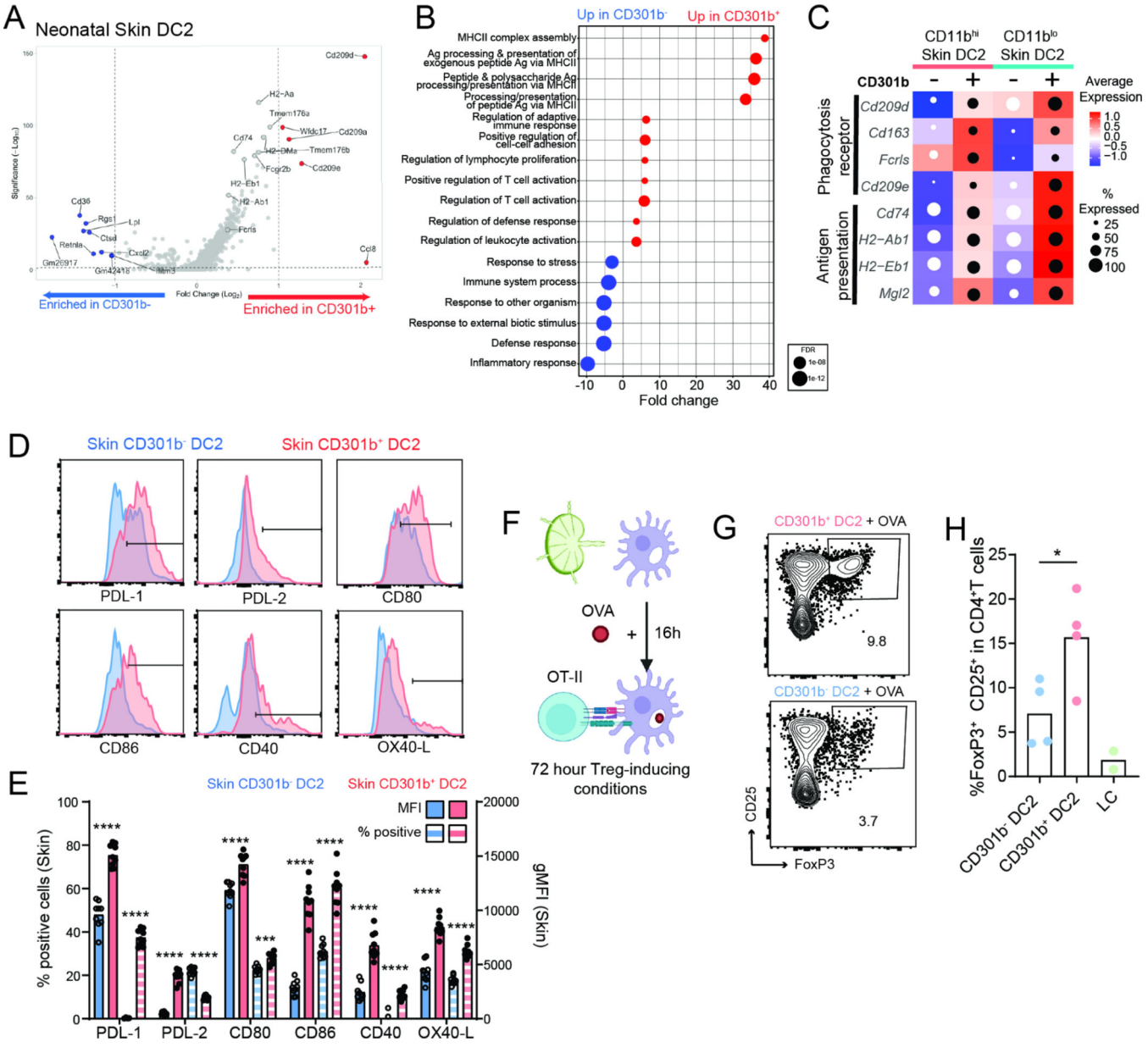

Figure 4: Expression of CD301b delineates a subgroup of DC2 enriched in phagocytic, maturation as well as regulatory markers

(A) Top differentially expressed genes by scRNAseq in CD301b$^+$ vs. CD301b$^-$ DC2 in D10 murine skin, complete list in Table S1. (B) Central functions enriched in each subset based on pathway analysis, complete list in Table S2. (C) Heat map of normalized average expression (box color) and percentage of expressing cells (circle size) for indicated genes in CD301b$^+$ vs. CD301b$^-$ cells in either CD11b^{hi} or CD11b^{lo} DC2 clusters. Genes shown had p-value <0.05 in two independent scRNAseq experiments. (D-E) Spectral flow cytometry of activation markers in CD301b$^+$ vs. CD301b$^-$ DC2 from D10 skin 16h after *S. epidermidis* colonization. (D) Representative histograms and gates used to delineate positive cells with corresponding (E) quantification of the % positive cells and geometrical mean of fluorescence intensity (gMFI) among positive cells for the indicated markers. Each dot

is a biological replicate. 1 of 2 independent experiments is shown. Two-way ANOVA. (F) CD301b^{+} or CD301b^{-} DC2 were sorted from D10 SDLN migDC, incubated overnight with OVA protein, then cultured with CTV-labelled OT-II plus IL-2 and TGF-β to measure DC Treg-promoting capacity. (G) Representative plots (pre-gating: Live CD4^{+}TCRβ^{+}) and (H) quantification of OT-II Treg cells at 72h, data pooled from 2–4 independent experiments. Student's paired t-test. *p < 0.05, **p < 0.01, ***p < 0.001, ****p<0.0001.

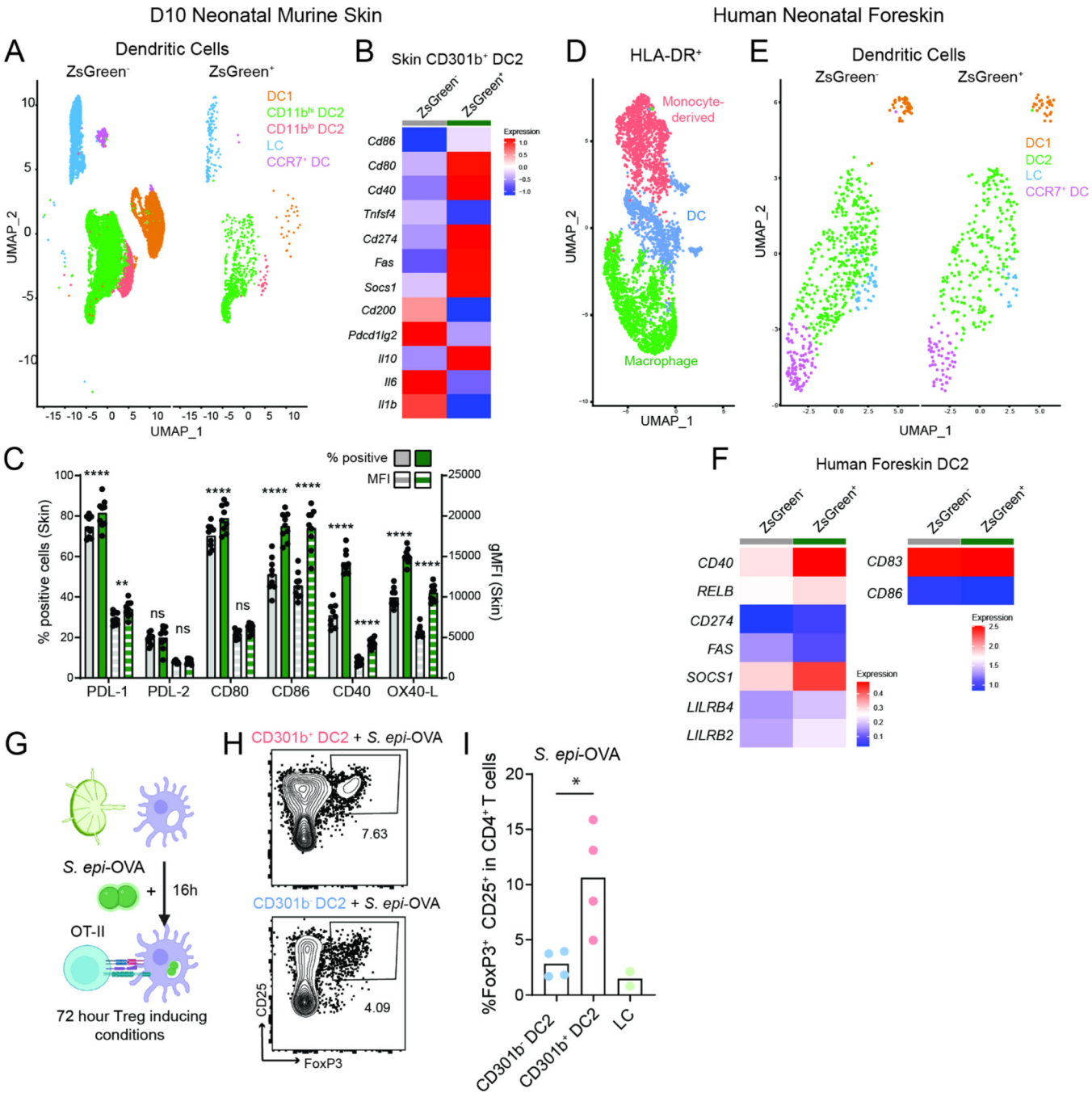

Figure 5: Maturation and tolerogenic features of murine and human neonatal skin DC2 are sustained upon commensal uptake

(A-B) Neonatal mice were colonized with *S. epi*-ZsGreen and skin was harvested 16h later, with commensal antigen-loaded (ZsGreen^{+}) and unloaded (ZsGreen^{-}) DCs separately sorted and submitted for scRNAseq. (A) UMAP of all ZsGreen^{+} vs. ZsGreen^{-} DCs. (B) Heatmap of select genes differentially expressed between ZsGreen^{+} vs. ZsGreen^{-} CD301b^{+} DC2 (CD301b status defined based on *Mgl2* expression). (C) Spectral flow cytometry of key markers both percent positive and gMFI on positive cells for ZsGreen^{+} vs. ZsGreen^{-} CD301b^{+} DC2 in neonatal skin 16h after *S. epi*-ZsGreen colonization. Each dot is a

biological replicate. 1 of 2 independent experiments. Two-way ANOVA. (D-F) Human neonatal foreskin was incubated 4h with *S. epi*-ZsGreen then live ZsGreen^{+} and ZsGreen^{-} CD45^{+}CD16^{-} HLADR^{+} cells were separately sorted and submitted for scRNAseq. (D) UMAP of all cells combined, (E) UMAP of DC clusters split by ZsGreen status, and (F) heatmaps comparing expression of select genes between ZsGreen^{+} and ZsGreen^{-} DC2. (G) CD301b^{+} or CD301b^{-} DC2 were sorted from D10 SDLN migDC, incubated overnight with *S. epi*-OVA, then cultured with CTV-labelled OT-II plus IL-2 and TGF-β to measure DC Treg-promoting capacity. (H) Representative plots (pre-gating: Live CD4^{+}TCRβ^{+}) and (I) and quantification of OT-II Treg cells at 72h. Each dot represents a biological replicate of DCs pooled from independent groups of neonatal mice, data pooled from 2–4 independent experiments. Student's unpaired t-test. *p < 0.05, **p < 0.01, ***p < 0.001, ****p<0.0001, ns = not significant.

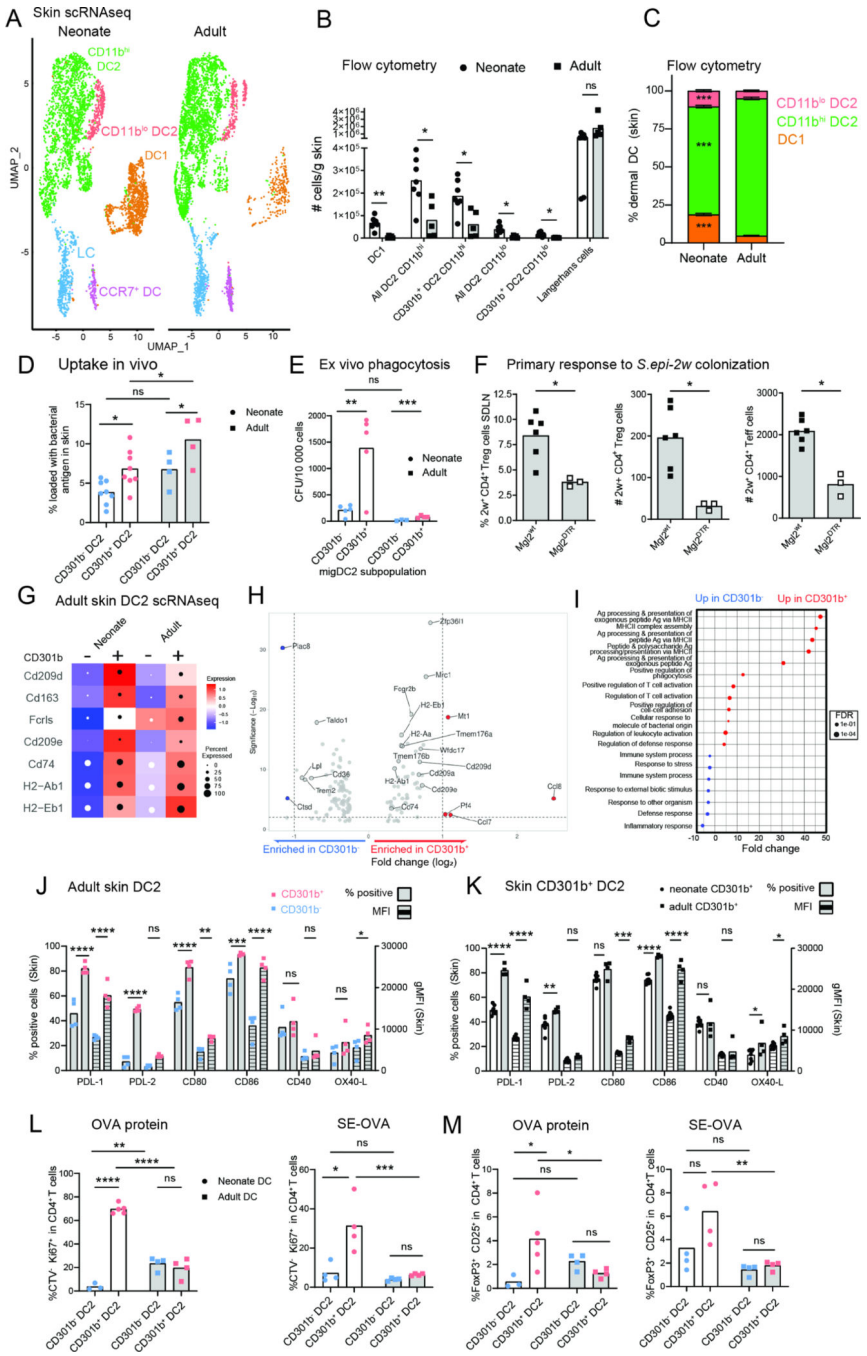

Figure 6: Characterization of adult versus neonatal skin CD301b$^+$ DC2

(A) Split UMAP of major DC populations in D10 (neonate) and 6-week-old (adult) murine skin from scRNAseq of sorted live MHCII$^+$CD11c$^+$ cells. (B-C) Flow quantification of dermal and epidermal DCs in D12 vs. adult skin. (B) Total cell numbers and (C) proportion of dermal DCs. (D) Percentage of ZsGreen$^+$ cells in neonatal or adult skin CD301b$^+$ and CD301b$^-$ DC2 16h after *S. epi*-ZsGreen colonization. (E) *S. epidermidis* uptake by neonatal or adult CD301b$^+$ and CD301b$^-$ SDLN migDC2 in ex vivo phagocytosis assay. (F) Primary response to *S. epi*-2w in adults. Percentage and total number of 2w$^+$ Treg cells

(left and middle) and $2w^+$ Teff cells (right). One of two independent experiments. (G-I) Comparison of $CD301b^+$ and $CD301b^-$ DC2 by scRNAseq. (G) Heatmap of normalized average expression (box color) and percentage of expressing cells (circle size) for indicated genes in adult and neonatal skin $CD301b^+$ and $CD301b^-$ DC2. All genes but *Fcrls* for adults have a p-value <0.05. (H) Top differentially expressed genes in $CD301b^+$ vs. $CD301b^-$ DC2 in adult skin, complete list in Table S4. (I) Central functions enriched in each subset based on pathway analysis, complete list in Table S5. (J-K) Spectral flow cytometry of activation markers in (J) adult skin $CD301b^+$ vs. $CD301b^-$ DC2 and (K) adult vs. D12 neonatal skin $CD301b^+$ DC2. Percent positive cells and geometrical mean of fluorescence intensity (gMFI) among positive cells are shown. (L-M) $CD301b^+$ or $CD301b^-$ migDC2 were sorted from D10 or adult SDLN and incubated with OVA protein (left) or *S. epi*-OVA (right) before 72h culture with neonatal OT-II in the presence of IL-2 and TGF-β. (L) Percent proliferating ($CTV^-Ki67^{+)}$ cells and (M) percent Treg cells at 72. Data from one of two replicate experiments. (B, D-F, J-M) each dot is separate biological replicate. Two-way ANOVA except in (F), Student's unpaired t-test. *p < 0.05, **p < 0.01, ***p < 0.001, ****p<0.0001, ns = not significant.

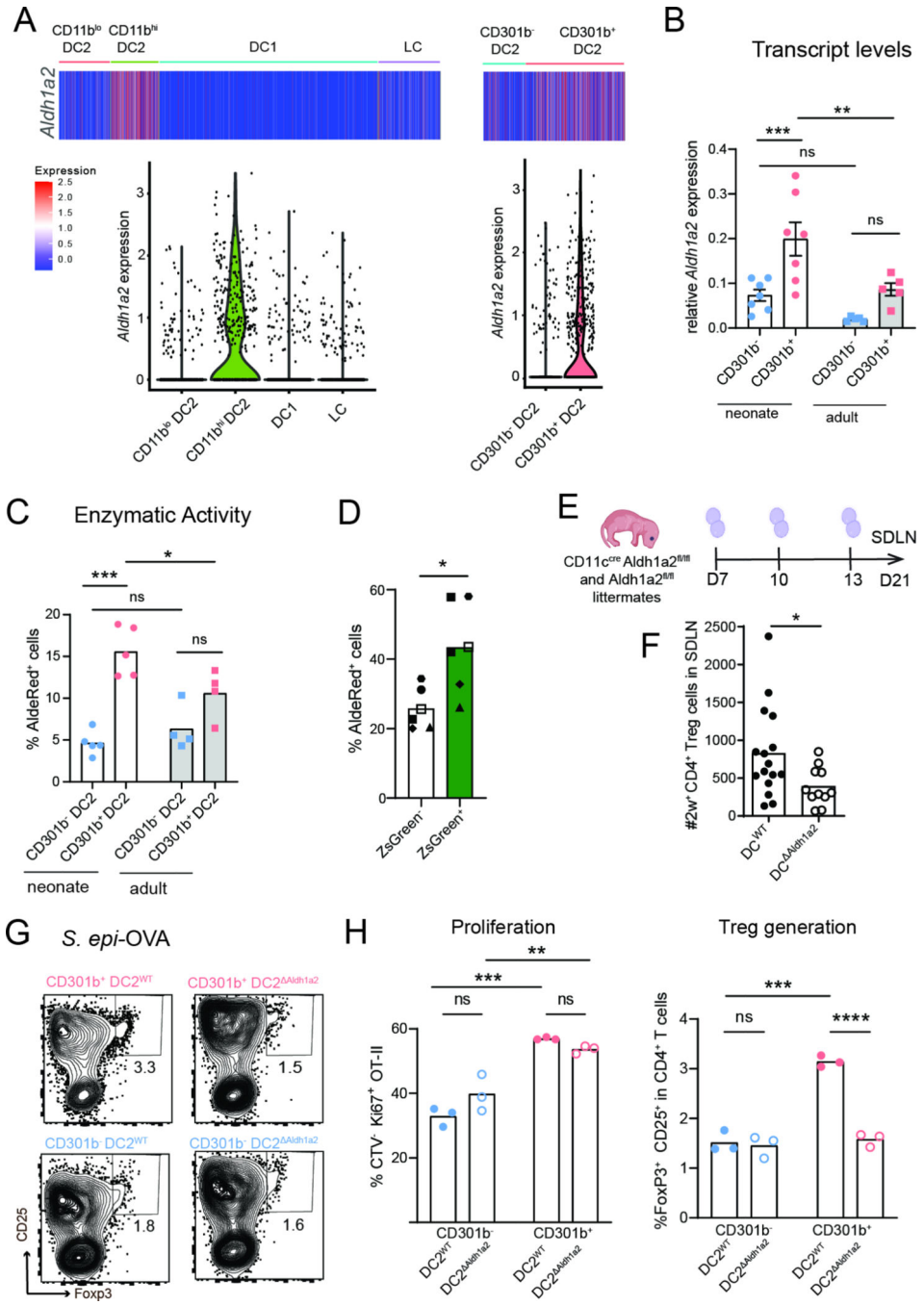

Figure 7: *Aldh1a2* expression is enriched in neonatal CD301b$^+$ DC2s and promotes generation of commensal-specific Treg cells

(A) Heatmap (top) and Violin Plot (bottom) of *Aldh1a2* expression in subpopulations of D10 SDLN migDC. (B) qRT-PCR of *Aldh1a2* expression and (C) ALDH enzymatic activity in CD301b$^+$ vs. CD301b$^-$ migDC2 sorted from SDLN of D10 or adult mice. Each dot is an independent mouse. (D) CD301b$^-$ migDC2 were sorted from neonatal SDLN and incubated for 16 with *S. epi*-ZsGreen. Enzymatic ALDH activity in ZsGreen$^+$ vs. ZsGreen$^-$ CD301b$^+$ DC2. Each dot represents a biological replicate of cells pooled from two mice. Wilcoxon test. (E) *Cd11c^{cre}Aldh1a2$^{fl/fl}$* and *Aldh1a2$^{fl/fl}$* littermates were colonized neonatally with *S.*

epi-2w then (F) total number $2w^+$ Treg cells in the SDLN were enumerated on D21. Mann-Whitney test. (G-H) $CD301b^+$ or $CD301b^-$ migDC2 were sorted from *Cd11c*^{cre} *Aldh1a2*$^{fl/fl}$ and *Aldh1a2*$^{fl/fl}$ D10 SDLN then incubated overnight with *S. epi*-OVA before 72h culture with OT-II in the presence of IL-2 and TGF-β. (G) Representative plots (pre-gating: Live $CD4^+TCR\beta^+$) and (H) quantification of OT-II Treg cells. One of three representative independent experiments shown. Dots indicate biological replicates from DCs sorted from pooled neonates. Two-way ANOVA unless specified. *$p < 0.05$, **$p < 0.01$, ***$p < 0.001$, ns = not significant.

Key resources table

REAGENT or RESOURCE	SOURCE	IDENTIFIER
Antibodies		
Per-Cp-Cy5.5 anti-mouse TCR-beta (clone H57-597)	BioLegend	Cat# 109228; RRID: AB_1575173
Per-Cp-Cy5.5 anti-mouse TCR-beta (clone H57-597)	BioLegend	Cat# 109228; RRID: AB_1575173
FITC anti-mouse/human Helios (clone 22F6)	BioLegend	Cat# 137214; RRID: AB_10662745
Pe-Cy7 anti-mouse CD8 (clone 53-6.7)	BD Biosciences	Cat# 552877; RRID: AB_394506
APC-efluor 780 anti-mouse B220 (clone RA3-6B2)	Thermo Fisher Scientific	Cat# 47-0452-80; RRID: AB_1518811
APC-efluor 780 anti-mouse CD11b (clone M1/70)	Thermo Fisher Scientific	Cat# 47-0112-82; RRID: AB_1603193
APC-efluor 780 anti-mouse CD11c (clone N4818)	Thermo Fisher Scientific	Cat# 47-0114-82; RRID: AB_1548652
APC-efluor 780 anti-mouse F4/80 (clone BM8)	Invitrogen	Cat# 47-4801-82; RRID: AB_2735036
APC anti-mouse CD44 (clone IM7)	Thermo Fisher Scientific	Cat# 17-0441-82; RRID: AB_469390
e450 anti-mouse Foxp3 (clone FJK-16S)	Thermo Fisher Scientific	Cat#48-5773-82; RRID: AB_1518812
BV650 anti-mouse CD4 (clone RM4-5)	BD Biosciences	Cat#563747; RRID: AB_2716859
PE/Cyanine7 anti-mouse IL-17A (clone TC11-18H10.1)	BioLegend	Cat# 506922; RRID:AB_2125010
PE anti-mouse CD8a (clone 53-6.7)	Thermo Fisher Scientific	Cat# 56-0081-80; RRID:AB_494006
BV480 Rat Anti-Mouse CD8a (Clone 53-6.7)	BD Biosciences	Cat# 566096; RRID:AB_2739500
BV605 anti-mouse TCR-beta (clone H57-597)	BD Biosciences	Cat# 562840; RRID: AB_2687544
BV711 anti-mouse CD3 (clone 145-2C11)	BD Biosciences	Cat#563123; RRID: AB_2687954
PerCP/Cyanine5.5 anti-mouse CD301b (clone URA-1)	BioLegend	Cat# 146810; RRID:AB_2563392
PE/Cyanine7 anti-mouse Ly-6G (clone 1A8)	BioLegend	Cat# 127618; RRID:AB_1877261
PE anti-mouse/human CD11b (clone M1/70)	BioLegend	Cat# 101208; RRID:AB_312791
APC anti-mouse CD103 (clone 2E7)	Thermo Fisher Scientific	Cat# 17-1031-82; RRID: AB_1106992
e450 anti-mouse MHCII (clone M5/114.15.2)	Thermo Fisher Scientific	Cat#48-5321-82; RRID: AB_1272204
BV605 anti-mouse Ly6C (clone HK1.4)	BioLegend	Cat#128035; RRID: RRID:AB_2562352
Brilliant Violet 650™ anti-mouse CD326 (Ep-CAM) (clone G8.8)	BioLegend	Cat# 118241; RRID:AB_2876432
BV786 anti-mouse CD64 (clone X54-5/7.1)	BD Biosciences	Cat#741024; RRID:AB_2740644
FITC Rat Anti-Mouse CD25 (clone 7D4)	BD Biosciences	Cat# 553072; RRID:AB_394604
PE-Cy™7 Mouse anti-Ki-67 (clone B56)	BD Biosciences	Cat# 561283; RRID:AB_10716060
PE anti-mouse CD69 (clone H1.2F3)	BioLegend	Cat# 104507; RRID:AB_313110
Alexa Fluor™ 700 anti-mouse CD3 (clone 17A2)	Thermo Fisher Scientific	Cat# 56-0032-82; RRID:AB_529507
AlexaFluor700 anti-mouse CD45 (clone 30-F11)	Thermo Fisher Scientific	Cat# 56-0451-82; RRID:AB_891454
APC anti-mouse FOXP3 (clone FJK-16s)	Thermo Fisher Scientific	Cat# 17-5773-82; RRID:AB_469457
Brilliant Violet 785™ anti-mouse CD8a (clone 53-6.7)	BioLegend	Cat# 100749; RRID:AB_11218801
PerCP/Cyanine5.5 anti-mouse TCR γ/δ (clone GL3)	BioLegend	Cat# 118118; RRID:AB_10612756
BUV395 Rat Anti-Mouse I-A/I-E (Clone 2G9)	BD Biosciences	Cat# 743876; RRID:AB_2741827
BUV496 Rat Anti-Mouse CD45 (clone 30-F11)	BD Biosciences	Cat# 749889; RRID:AB_2874129
BUV805 Rat Anti-CD11b (Clone M1/70)	BD Biosciences	Cat# 741934; RRID:AB_2871246
BV480 Hamster Anti-Mouse CD11c (clone N418)	BD Biosciences	Cat# 746392; RRID:AB_2743706

REAGENT or RESOURCE	SOURCE	IDENTIFIER
Alexa Fluor® 594 anti-mouse CD103 (clone 2E7)	BioLegend	Cat# 121428; RRID:AB_2565571
PE Rat Anti-Mouse CD40 (clone 3/23)	BD Biosciences	Cat# 561846; RRID:AB_10896482
PE/Cyanine7 anti-mouse CD252 (OX40L) (clone RM134L)	BioLegend	Cat# 108813; RRID:AB_2565744
BUV737 Rat Anti-Mouse CD274 (PDL-1) (clone MIH5)	BD Biosciences	Cat# 741877; RRID:AB_2871203
APC Rat anti-Mouse CD273 (PDL-2) (clone TY25)	BD Biosciences	Cat# 560086; RRID:AB_1645223
BV750 Rat Anti-Mouse CD86 (clone GL1)	BD Biosciences	Cat# 747439; RRID:AB_2872120
BV421 Hamster Anti-Mouse CD80 (clone 16-10A1)	BD Biosciences	Cat# 562611; RRID:AB_2737675
Brilliant Violet 605™ anti-mouse CD197 (CCR7)	BioLegend	Cat# 120125; RRID:AB_2715777
PE-Cy7 anti-mouse CD11c (clone HL3)	BD Biosciences	Cat# 558079; RRID: AB_647251
TotalSeq™-A0201 anti-mouse CD103 (clone 2E7)	BioLegend	Cat# 121437; RRID:AB_2750349
TotalSeq™-A0014 anti-mouse/human CD11b (clone M1/70)	BioLegend	Cat# 101265; RRID:AB_2734152
TotalSeq™-A0566 anti-mouse CD301b (MGL2) (clone URA-1)	BioLegend	Cat# 146817; RRID:AB_2783115
PE/Cy7 Anti-human CD1c (clone: L161)	BioLegend	Cat# 331516;RRID:AB_2275574
PerCP/Cyanine5.5 anti-human HLA-DR (Clone Tü36)	BioLegend	Cat# 361608; RRID:AB_2563198
PE anti-human CD14 (clone M5E2)	BioLegend	Cat# 301806;RRID:AB_314188
APC-eFluor™ 780 anti-human CD45 (clone HI30)	Thermo Fisher Scientific	Cat# 47-0459-42; RRID:AB_1944368
A700 anti-human CD1a (clone H1149)	BioLegend	Cat# 300120;RRID:AB_528764
APC anti-human CD141 (Clone BDCA-3)	Miltenyi Biotech	Cat# 130-113-314;RRID:AB_2733313
BV605 anti-human CD11c (Clone B-Ly6)	BD Biosciences	Cat# 563929;RRID:AB_2744276
BV421 anti-human CD16 (clone 3G8)	BioLegend	Cat# 302038;RRID:AB_2561578
PE-conjugated 2w-loaded I-A(b) Tetramer	Provided by James Moon	
Staphylococcus epidermidis Tü3298	Provided by Michael Otto (Augustin and Gotz, 1990)	
Staphylococcus lugdunensis Slug_2E06	Provided by Julie Segre	
Staphylococcus hominis SK119	BEI	
Staphylococcus capitis Scap_DM02D06	Provided by Julie Segre	
Biological samples		
Healthy baby Foreskin tissue	UCSF Benioff Children's Hospital San Francisco	
Chemicals, peptides, and recombinant proteins		
PE-conjugated 2w-loaded I-A(b) Tetramer	Provided by James Moon	
Fetal bovine serum	Fisher scientific	Cat#SH3054103
Fetal calf serum	Fisher scientific	Cat#SH3007303
Tryptic Soy Medium	BD-Bacto	Cat#211825
Collagenase from *Clostridium* histolyticum, Type XI	Sigma-Aldrich	Cat#C9407
Collagenase from *Clostridium* histolyticum, Type I	Sigma-Aldrich	Cat#SCR103
Collagenase from *Clostridium* histolyticum, Type IV	Sigma-Aldrich	Cat#lS00418
Recombinant Human TGF-β1	Peprotech Inc.	Cat# 100-21C-10UG
Recombinant Murine IL-2	GoldBio	Cat#1310-02-100
Collagenase D	Sigma-Aldrich	Cat#11088866001

REAGENT or RESOURCE	SOURCE	IDENTIFIER
Diphtheria toxin	Sigma-Aldrich	Cat# D0564
Cytochalasin D	Cayman Chemicals	Cat#11330
Collagen I, rat tail	Thermo Fischer Scientific	Cat# A1048301
DNase	Sigma-Aldrich	Cat#DN25
Hyaluronidase from bovine testes	Sigma-Aldrich	Cat#H3506
Critical commercial assays		
Ghost Dye™ Violet 510 Live/Dead Stain	Tonbo Biosciences	Cat#13-0870-T100
EasySep™ Mouse PE Positive Selection Kit	StemCell Technologies	Cat#18554
CellTrace™ Violet Cell Proliferation Kit, for flow cytometry	Thermo Fischer Scientific	Cat# C34557
ViaDye Red	Cytek	R7-60008
Ghost Dye™ Violet 780 Live/Dead Stain	Tonbo Biosciences	Cat#13-0865-T100
Allprep DNA/RNA micro kit	Qiagen	Cat# 80284
SuperScript™ III First-Strand Synthesis System	Thermo Fischer Scientific	Cat# 18080051
Buffer RLT Plus	Qiagen	Cat# 1053393
Power SYBR Green PCR master mix	Thermo Fischer Scientific	Cat#4368577
AldeRed® ALDH Detection Assay	Sigma-Aldrich	Cat#SCR150
Mouse FoxP3 Buffer Set	eBiosciences	Cat#00-5523-00
Deposited data		
Mouse neonatal dendritic cells from uncolonized, and Staphylococcus epidermidis-zsgreen colonized mouse (loaded and non-loaded cells	This paper	GSE206891
Skin and Skin Draining lymph node dendritic cells from neonatal mouse colonized with a commensal or control	This paper	GSE206892
Neonatal foreskin antigen presenting cells after colonization with Staphylococcus epidermidis	This paper	GSE206893
Adult mouse skin dendritic cells	This paper	GSE217891
Experimental models: Cell lines		
Experimental models: Organisms/strains		
SPF C57BL/6J mice	Jackson Laboratory	Cat#000664
$Mgl2^{Cre}H2ab1^{fl/f}$	Provided by Y. Kumamoto	
$Cd11c^{Cre}$ $Aldh1a2^{fl/f}$	Provided by R. Noelle	
$Xcr1^{DTR\text{-}Venus}$	Jackson Laboratory	Cat#5544058
OT-II	Jackson Laboratory	Cat#004194
$HuLang^{DTR}$	Provided by D. Kaplan	
$Mgl2^{DTR\text{-}eGFP}$	Provided by Y. Kumamoto	
Oligonucleotides		
Aldh1a2 primer forward: 5'-GACTTGTAGCAGCTGTCTTCACT-3'		
Aldh1a2 primer reverse: 5'-TCACCCATTTCTCTCCCATTTCC-3'		
Rsp17 forward: ATTGAGGTGGATCCCGACAC		

REAGENT or RESOURCE	SOURCE	IDENTIFIER
Rsp17 reverse: TGCCAACTGTAGGCTGAGTG		
Recombinant DNA		
ZsGreen optimized for expression in *Staphylococcus* to generate pJL74-2w-zsgreen	DNA 2.0/ATUM	Custom project
Software and algorithms		
GraphPad Prism	GraphPad Software, Inc	http://www.graphpad.com/scientific-software/prism/
FlowJo v10.5.0	FlowJo, LLC	https://www.flowjo.com/solutions/flowjo
Seurat	Stuart T. et al. 2019	
R Statistical Computing Software	The R Foundation	https://www.r-project.org/
Other		
World Precision Instrument Low Toxicity Silicone Adhesive, 2 5ml Syringes	Fischer scientific	50-822-154